Supporting Information for

Theoretical Investigation into the Position-dependent Influence of L-Deoxynucleotides in the Template on T7 RNA Polymerase Transcription Activity

Xuyang Ma[1,‡], Yongqi Ke[1,‡], Xinping Feng[1], Yang Zhang[1], Qingju Liu[3], Yujian He[1], Wei Cui[1,*] and Li Wu[1,2,*]

[1] School of Chemical Sciences, University of Chinese Academy of Sciences, Beijing, 100049, China

[2] State Key Laboratory of Natural and Biomimetic Drugs, School of Pharmaceutical Sciences, Peking University, Beijing, 100191, China

[3] Beijing Research Center for Agriculture Standards and Testing, Beijing Academy of Agriculture and Forestry Sciences, Beijing 100097, China

Experimental results for T7 RNA Polymerase Transcription reactions.

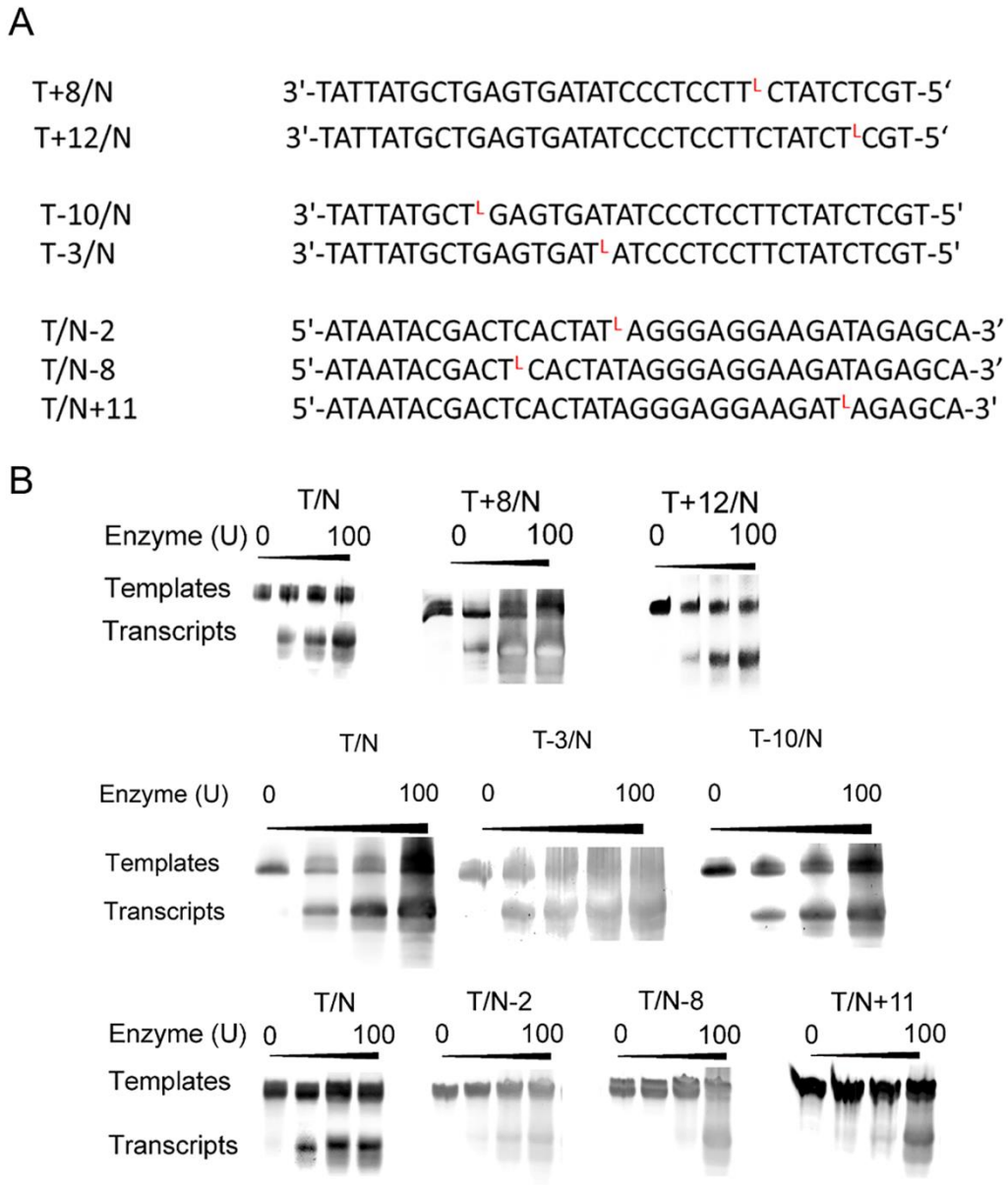

Figure S1 Experimental results for T7 RNA polymerase transcription reactions. (A) Sequences of templates used in the study. (B) PAGE of products of transcripts from templates containing $_{L}$-T at different positions of transcribed region and non-transcribed region in template strand and non-template region. The amount of T7 RNAP of four lanes with the same template were 0, 25, 50 and 100 U/mL, respectively. Templates concentrations of each lane was 1 μM. The position of the migration of the DNA templates and the RNA products were marked on the left on the gel. The DNA template used in each reaction is indicated at the top of each lane.

The free energy of the pre-insertion complex containing L-deoxynucleotides on the template

Table S1a The decomposition of free energies (kcal/mol) for the different via the Molecular Mechanics/Generalized Born Surface Area (MM/GBSA) method in complexes containing dT and L-dT.

dT (rNTP)	dT (rATP)	dT (rCTP)	dT (rGTP)	dT (rUTP)
Polar Energy (kcal/mol)	18.9383	17.2422	13.2431	14.9338
Non-Polar Energy (kcal/mol)	-70.0154	-56.4704	-61.2738	-49.0185
Binding Energy (kcal/mol)	-51.0771	-39.2282	-36.4158	-34.0847

L-dT (rNTP)	L-dT (rATP)	L-dT (rCTP)	L-dT (rGTP)	L-dT (rUTP)
Polar Energy (kcal/mol)	11.6405	12.6848	17.1206	13.8137
Non-Polar Energy (kcal/mol)	-53.8228	-41.7718	-46.8455	-44.3234
Binding Energy (kcal/mol)	-42.1822	-29.0871	-29.7249	-30.5097

Table S1b The decomposition of free energies (in kcal/mol) for the different via the Molecular Mechanics/Generalized Born Surface Area (MM/GBSA) method in complexes containing dA and L-dA.

dA (rNTP)	dA (rUTP)	dA (rCTP)	dA (rGTP)
Polar Energy (kcal/mol)	13.0127	17.5285	18.0962
Non-Polar Energy (kcal/mol)	-45.1817	-65.9591	-46.6347
Binding Energy (kcal/mol)	-32.1689	-48.4306	-28.5385

L-dA (rNTP)	L-dA (rCTP)	L-dA (rGTP)	L-dA (rUTP)
Polar Energy (kcal/mol)	17.6028	19.6718	14.1629
Non-Polar Energy (kcal/mol)	-48.5069	-52.251	-58.4504
Binding Energy (kcal/mol)	-30.9042	-32.5792	-44.2875

Table S1c The decomposition of free energies (in kcal/mol) for the different via the Molecular Mechanics/Generalized Born Surface Area (MM/GBSA) method in complexes containing dC and $_{L}$-dC.

dC (rNTP)	dC (rGTP)	dC (rUTP)	dC (rATP)
Polar Energy (kcal/mol)	18.3318	14.9999	16.8197
Non-Polar Energy (kcal/mol)	-69.2211	-48.0167	-52.6013
Binding Energy (kcal/mol)	-50.8892	-33.0169	-35.7815

$_{L}$-dC (rNTP)	$_{L}$-dC (rUTP)	$_{L}$-dC (rGTP)	$_{L}$-dC (rATP)
Polar Energy (kcal/mol)	17.2529	14.1916	17.1518
Non-Polar Energy (kcal/mol)	-54.8484	-63.9468	-49.2016
Binding Energy (kcal/mol)	-37.5955	-49.7552	-32.0796

Table S1d The decomposition of free energies (in kcal/mol) for the different via the Molecular Mechanics/Generalized Born Surface Area (MM/GBSA) method in complexes containing dG and $_{L}$-dG.

dG (rNTP)	dG (rCTP)	dG (rUTP)	dG (rATP)
Polar Energy (kcal/mol)	16.9299	15.8726	18.1000
Non-Polar Energy (kcal/mol)	-68.1133	-47.9876	-55.0987
Binding Energy (kcal/mol)	-51.1834	-32.1125	-36.9987

$_{L}$-dG (rNTP)	$_{L}$-dG (rCTP)	$_{L}$-dG (rATP)	$_{L}$-dG (rUTP)
Polar Energy (kcal/mol)	13.2542	18.1779	16.3637
Non-Polar Energy (kcal/mol)	-57.1113	-57.2642	-46.3883
Binding Energy (kcal/mol)	-43.8572	-31.0864	-30.0245

The decomposition of the free energy of the pre-insertion complex which containing L-deoxynucleotides on the template

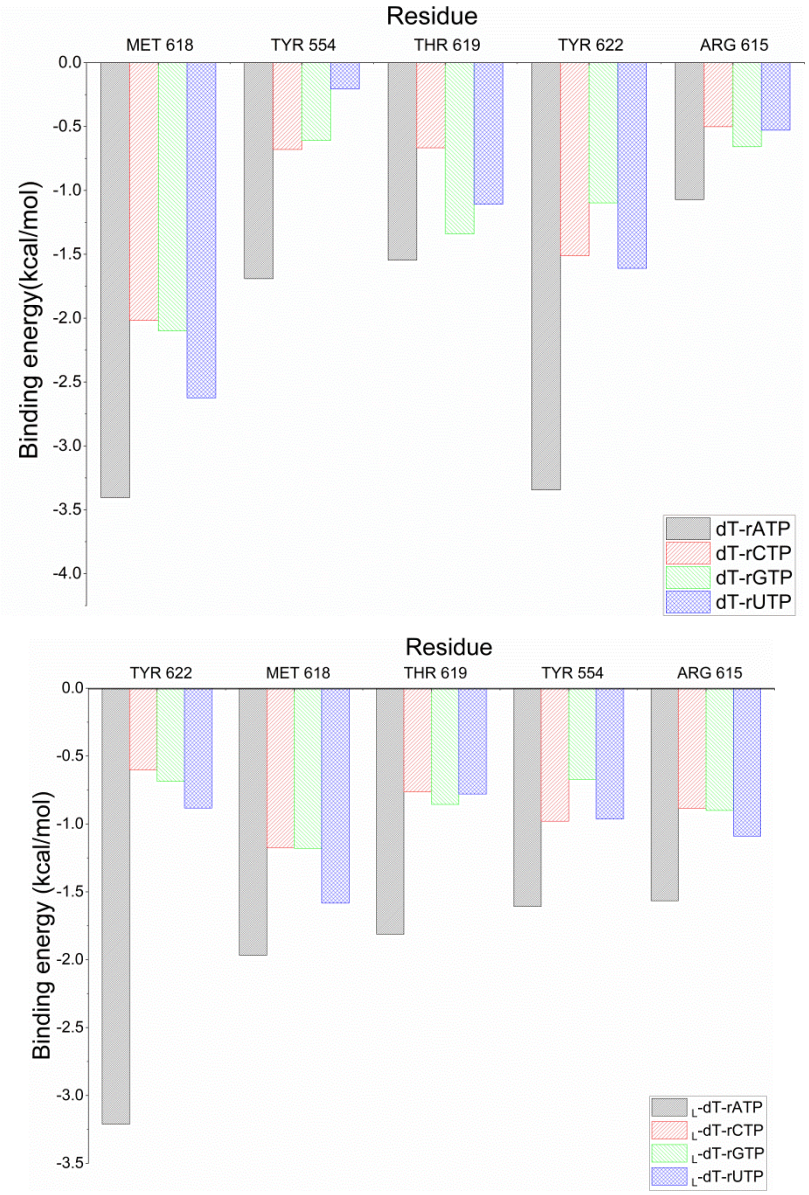

Figure S2a The decomposition of the free energy of residue in complexes containing dT and L-dT system**.**

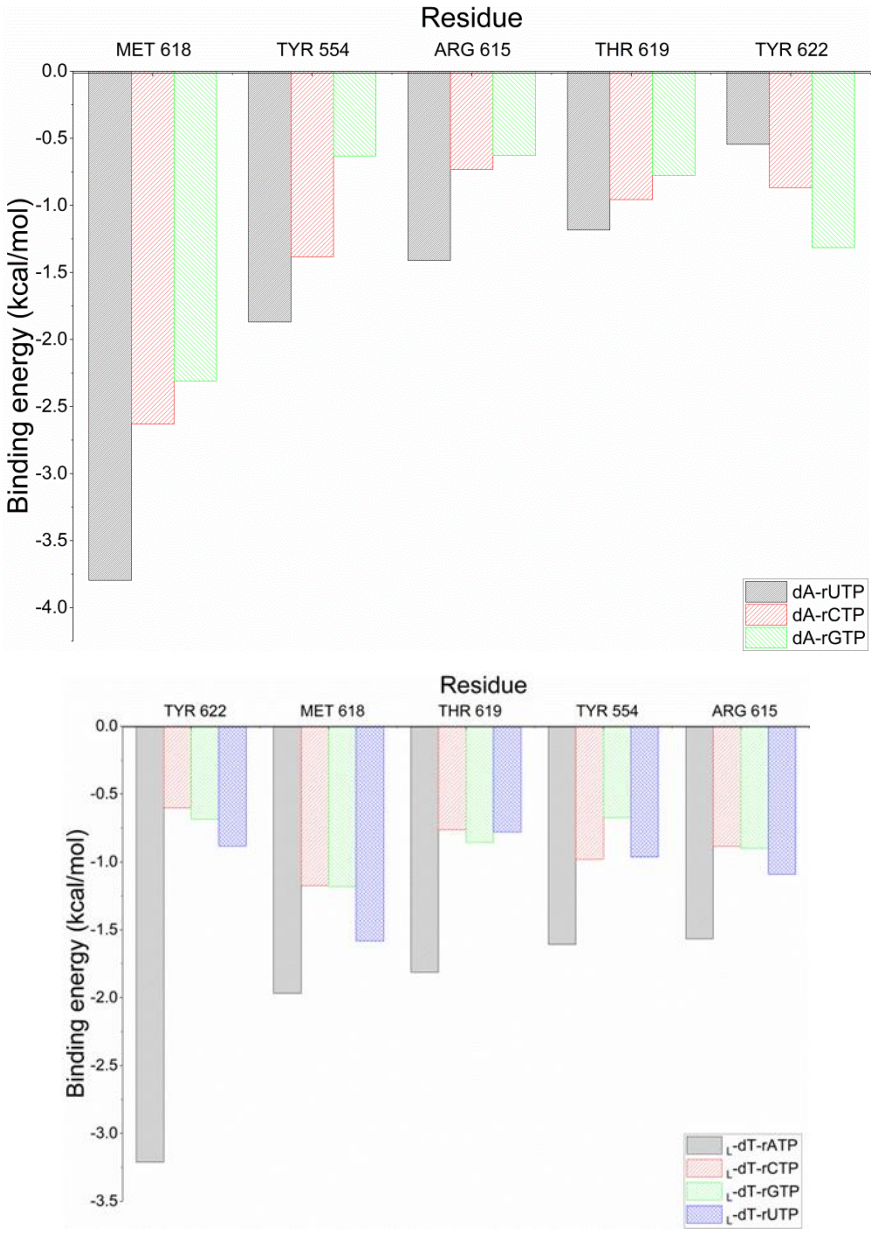

Figure S2b The decomposition of the free energy of residue in complexes containing dA and $_L$-dA system**.**

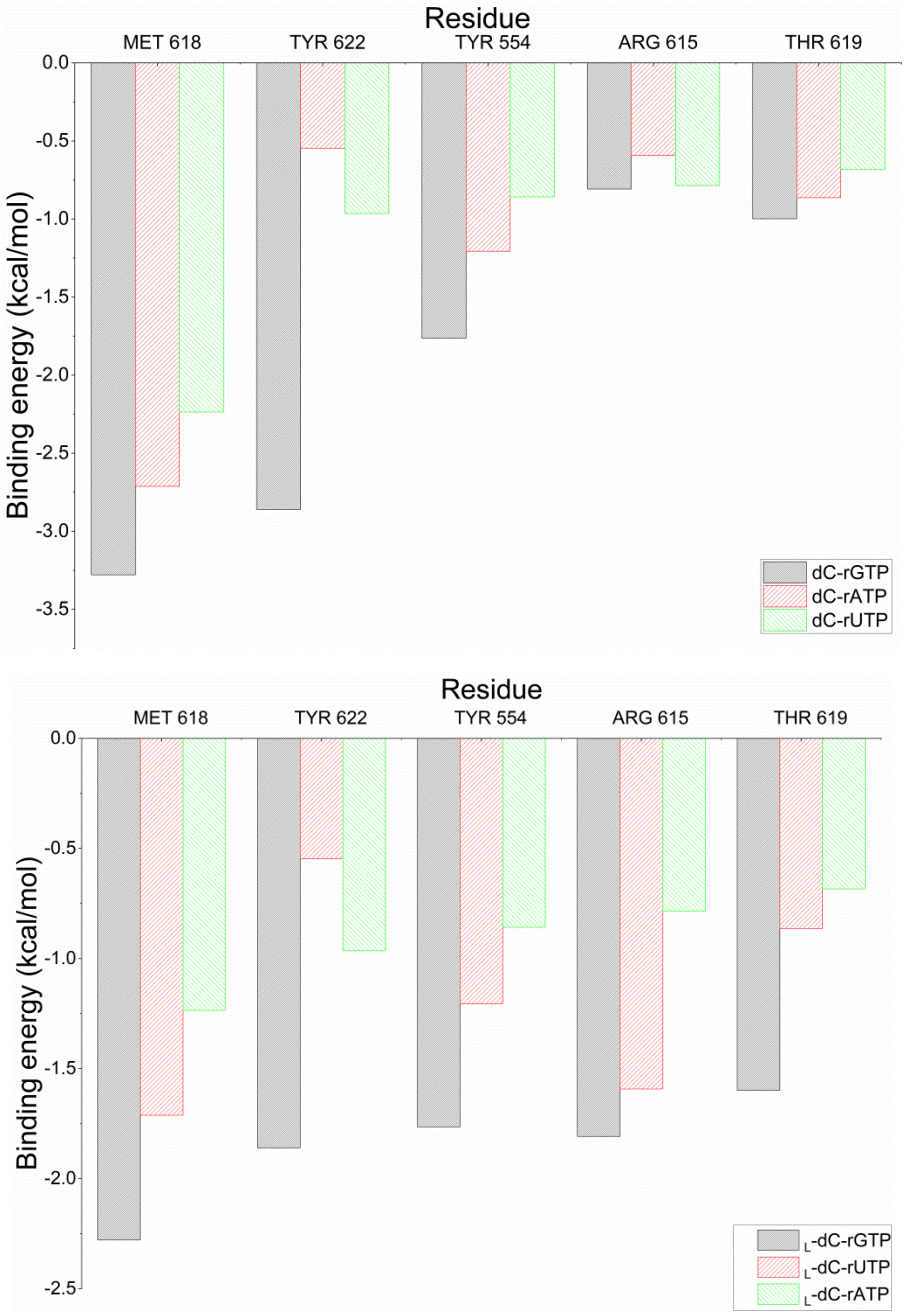

Figure S2c The decomposition of the free energy of residue in complexes containing dC and $_{L}$-dC system.

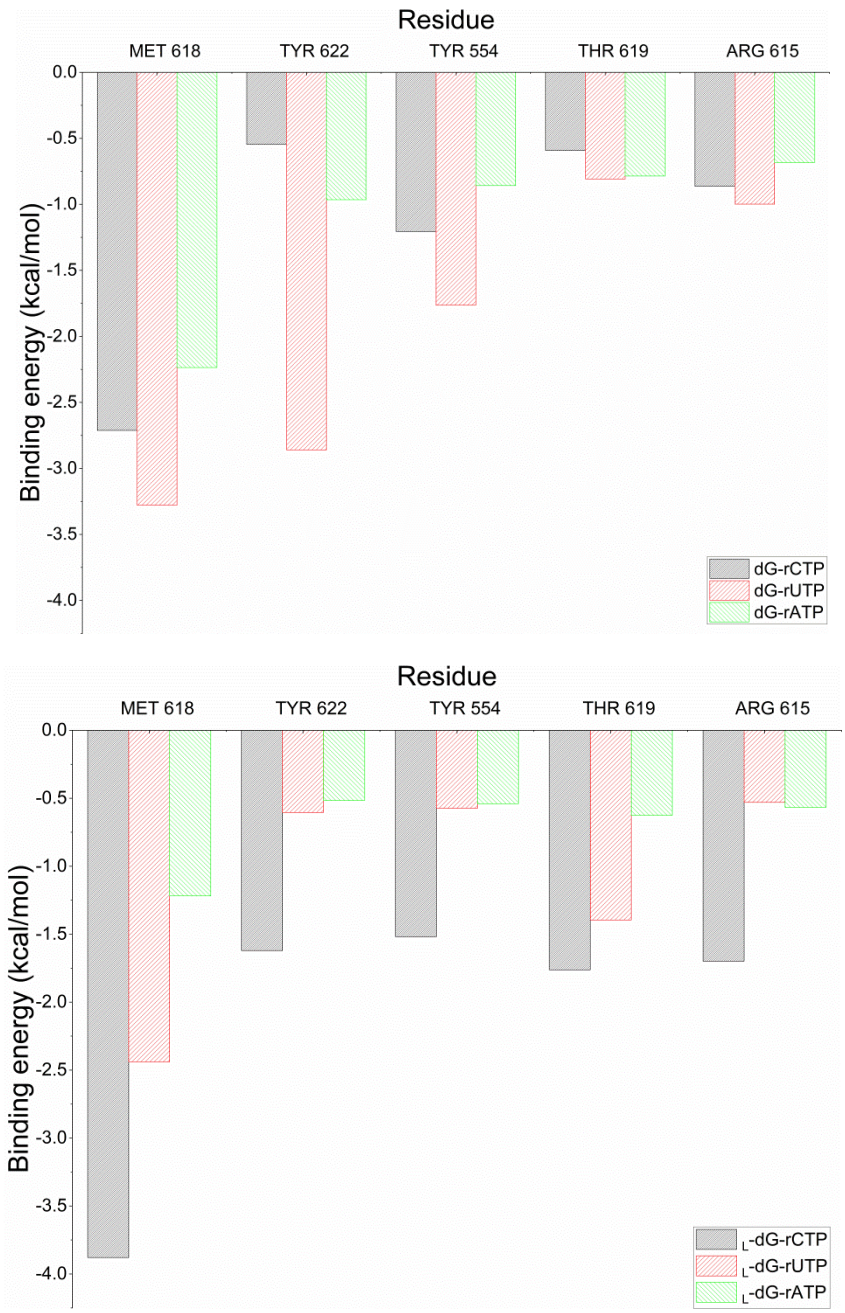

Figure S2d The decomposition of the free energy of residue in complexes containing dG and $_{L}$-dG system**.**

The RMSD values of O-helix in pre-translocation

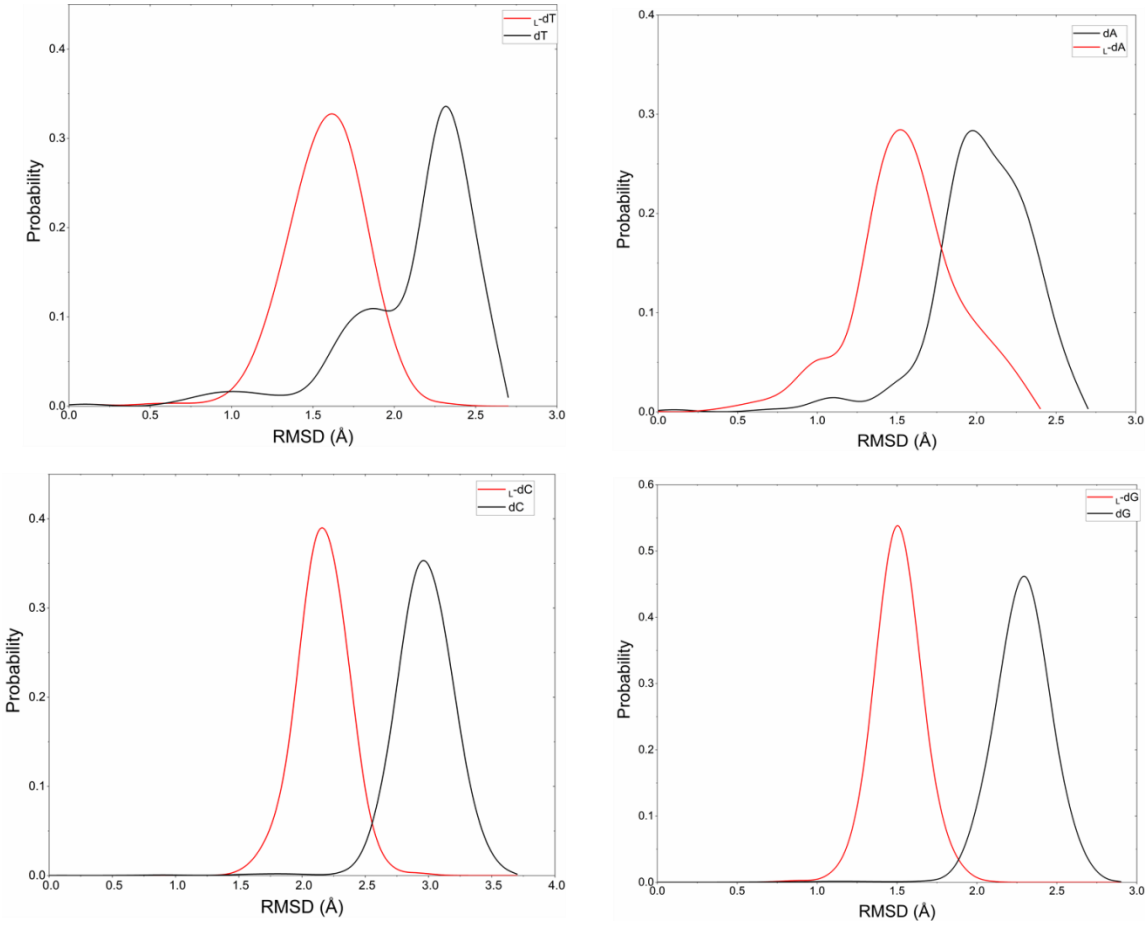

Figure S3 The RMSD values of O-helix of complexes containing L-deoxynucleotides in pre-translocation of T7 RNA polymerase.

The pseudorotation angles sampled by D- and L-deoxynucleotides in the template chain of DNA-RNA duplexes

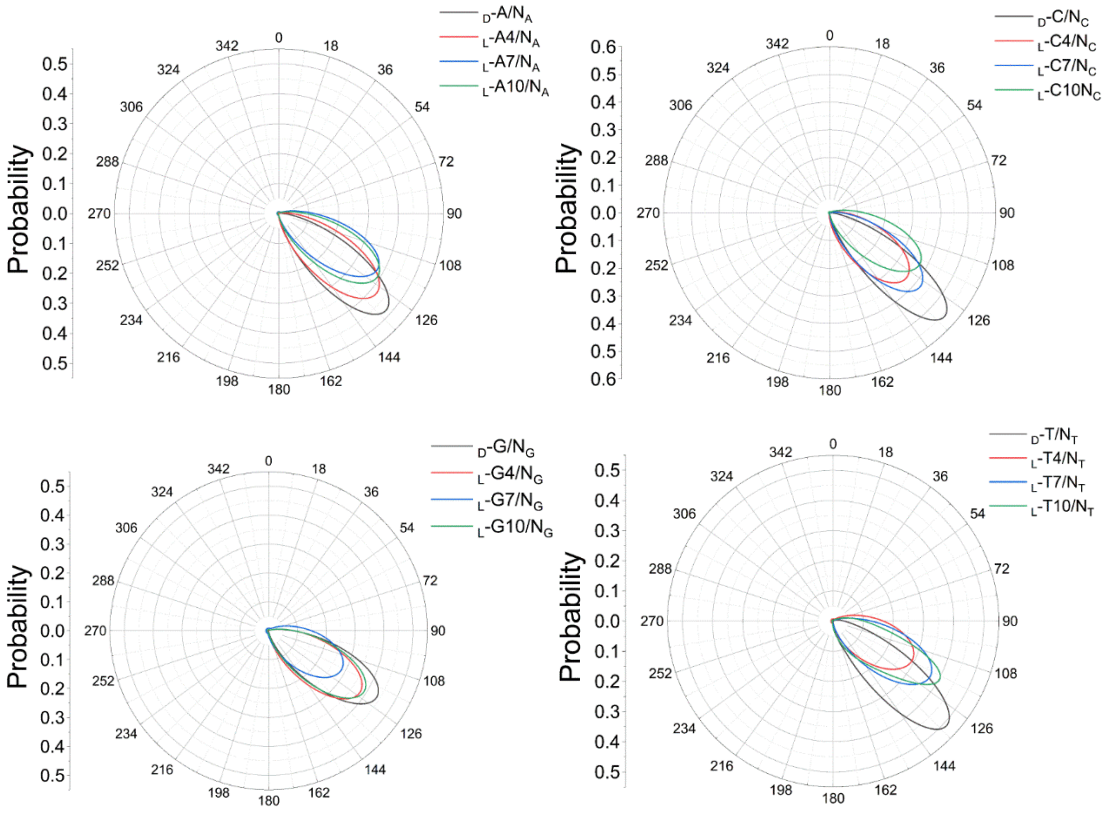

Figure S4 The pictorial representation of pseudorotation angles sampled by D- and L-deoxynucleotides in the template chain of DNA-RNA duplexes.

Probability distributions of the template backbone dihedral angles for L-dT, L-dA, L-dC, L-dG modified DNA/RNA duplexes

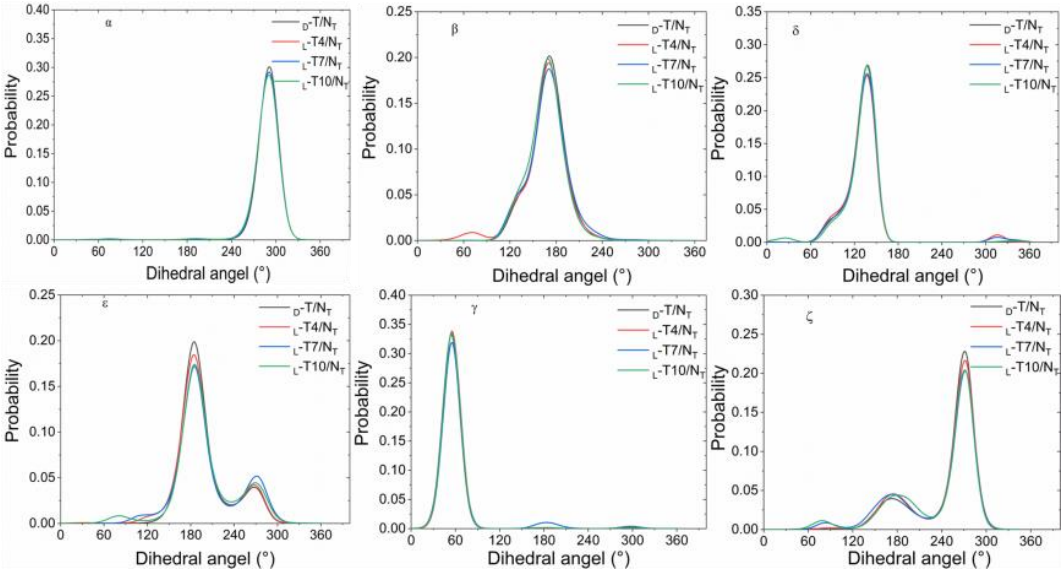

Figure S5a Probability distributions of backbone dihedral angles for the template of L-dT modified duplexes (L-T4/N_T, L-T7/N_T, L-T10/N_T) in comparison to nature DNA-RNA hybrid duplexes.

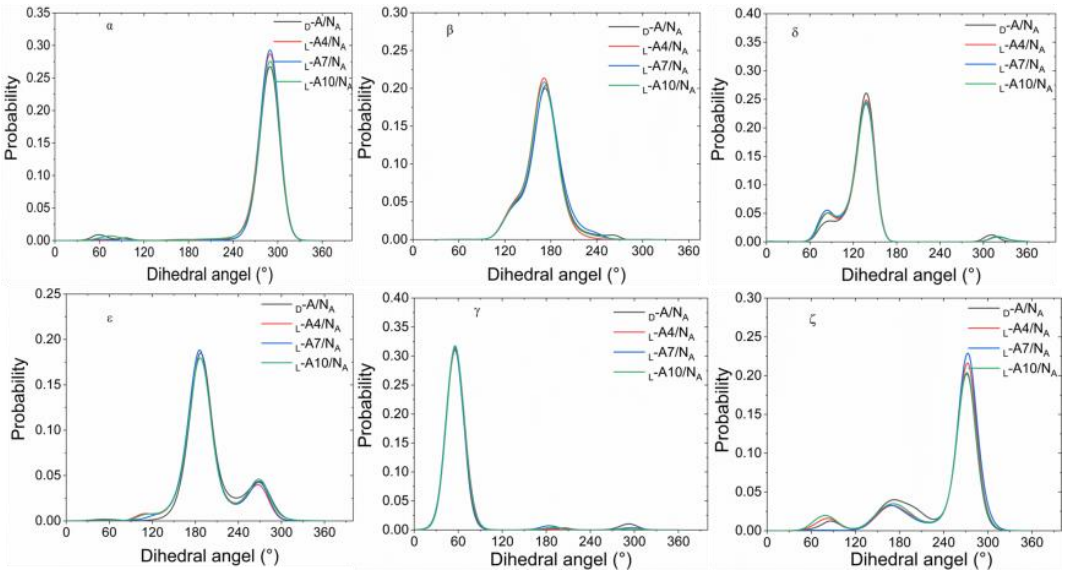

Figure S5b Probability distributions of backbone dihedral angles for the template of L-dA modified duplexes (L-A4/N_A, L-A7/N_A, L-A10/N_A) in comparison to nature DNA-RNA hybrid duplexes.

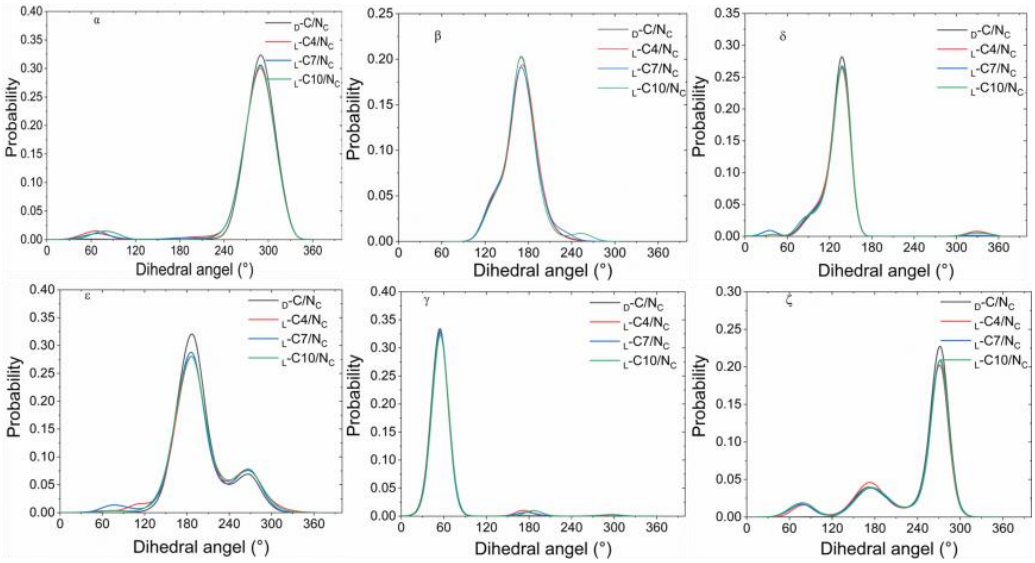

Figure S5c Probability distributions of backbone dihedral angles for the template of $_{L}$-dC modified duplexes ($_{L}$-C4/N$_{C}$, $_{L}$-C7/N$_{C}$, $_{L}$-C10/N$_{C}$) in comparison to nature DNA-RNA hybrid duplex.

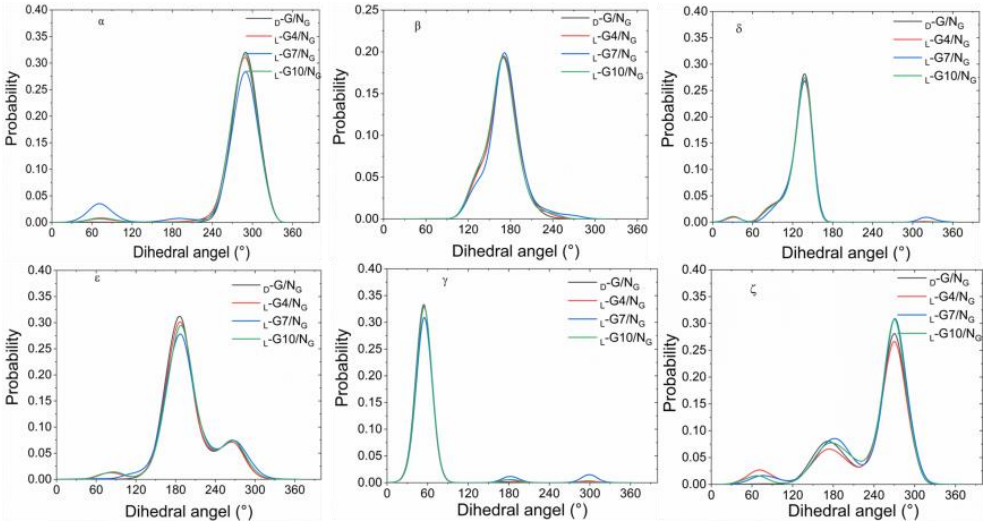

Figure S5d Probability distributions of backbone dihedral angles for the template of $_{L}$-dG modified duplexes ($_{L}$-G4/N$_{G}$, $_{L}$-G7/N$_{G}$, $_{L}$-G10/N$_{G}$) in comparison to nature DNA-RNA hybrid duplex.

The backbone dihedral angles of the surrounding nucleotides of L-deoxynucleotides of DNA/RNA hybrids and surrounding deoxynucleotides

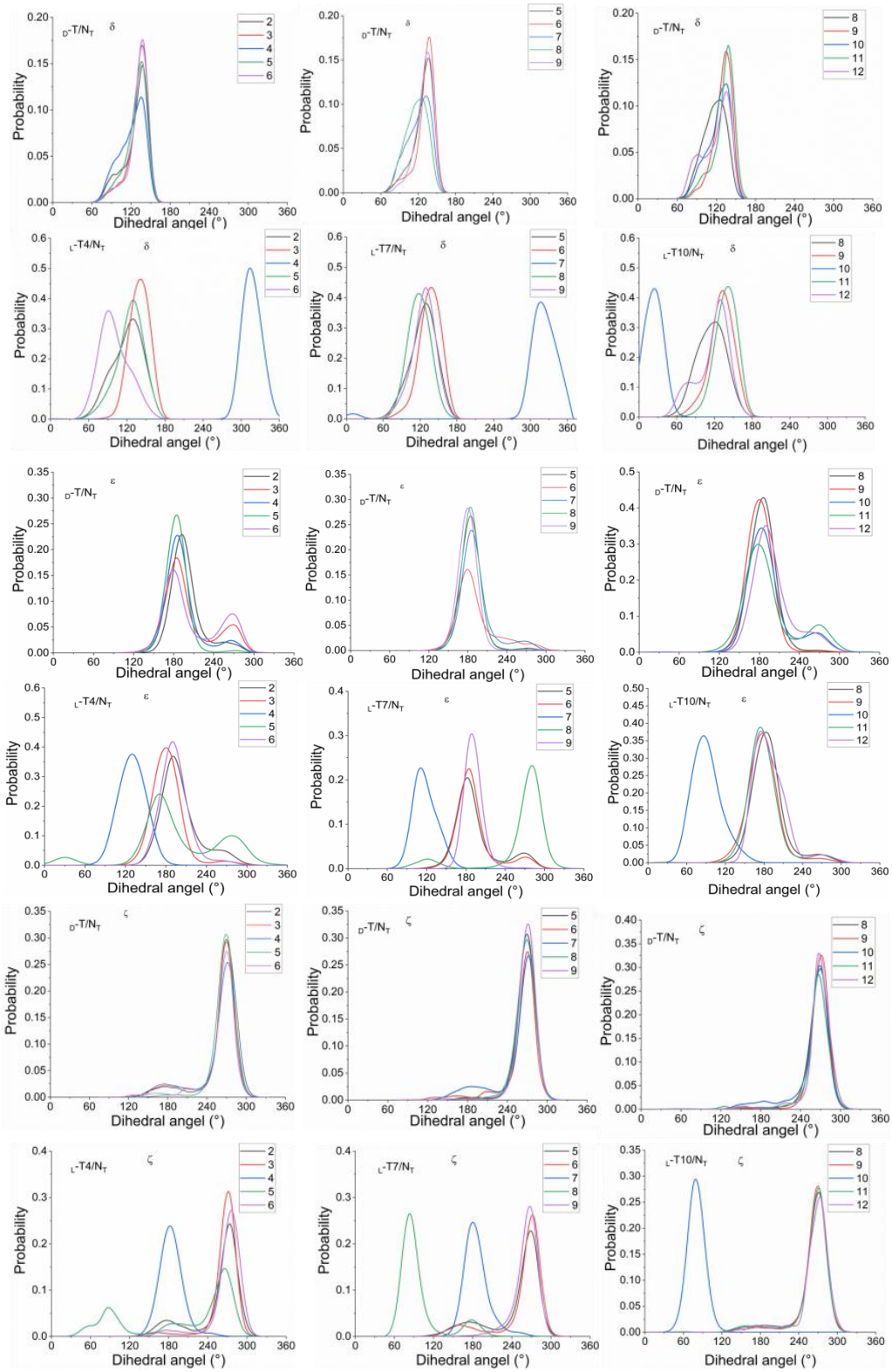

Figure S6a Probability distributions of dihedral angles for L-deoxynucleotides and surrounding deoxynucleotides in the L-dT4/N_T, L-dT7/N_T and L-dT10/N_T.

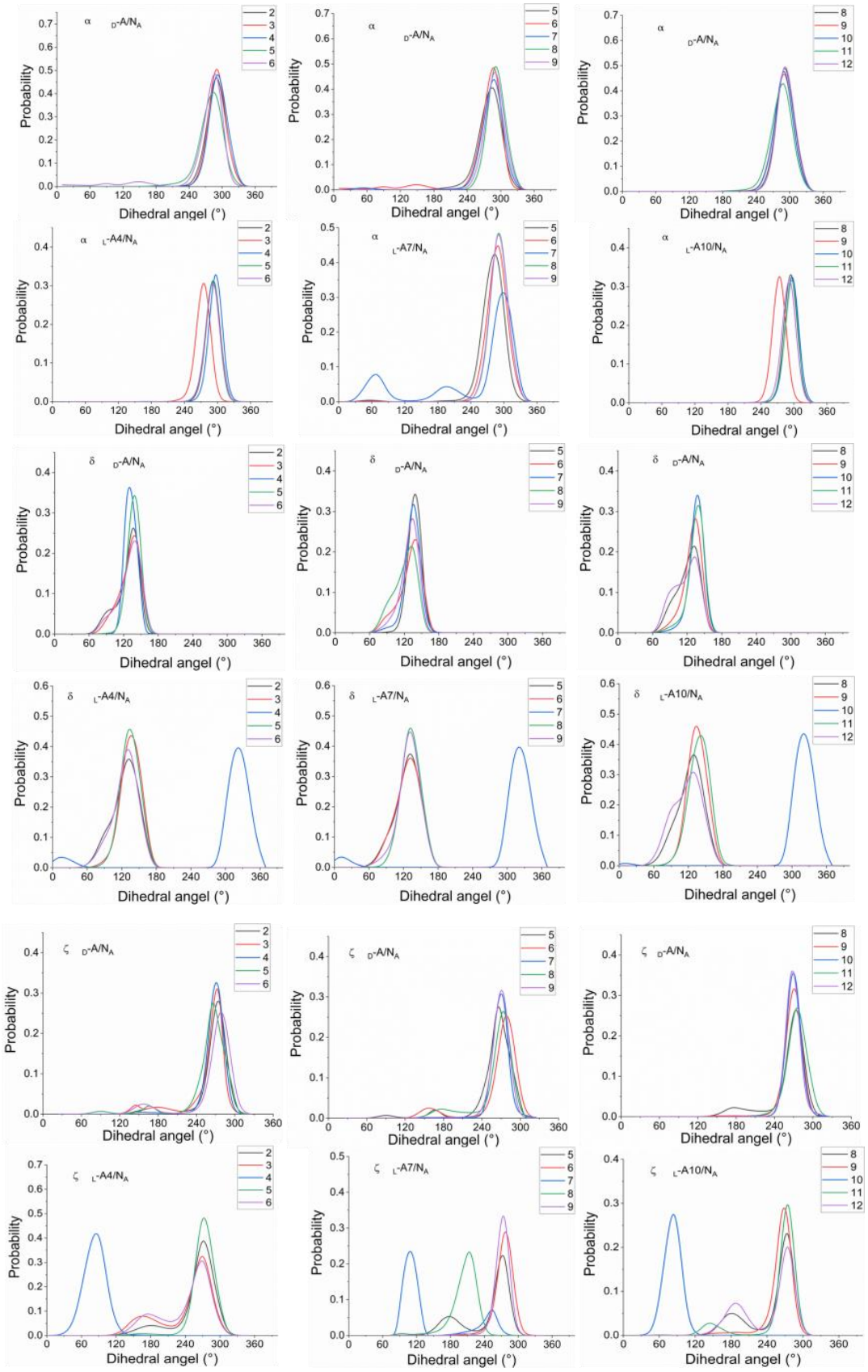

Figure S6b Probability distributions of dihedral angles for $_{L}$-deoxynucleotides and surrounding deoxynucleotides in the $_{L}$-dA4/N_A, $_{L}$-dA7/N_A and $_{L}$-dA10/N_A.

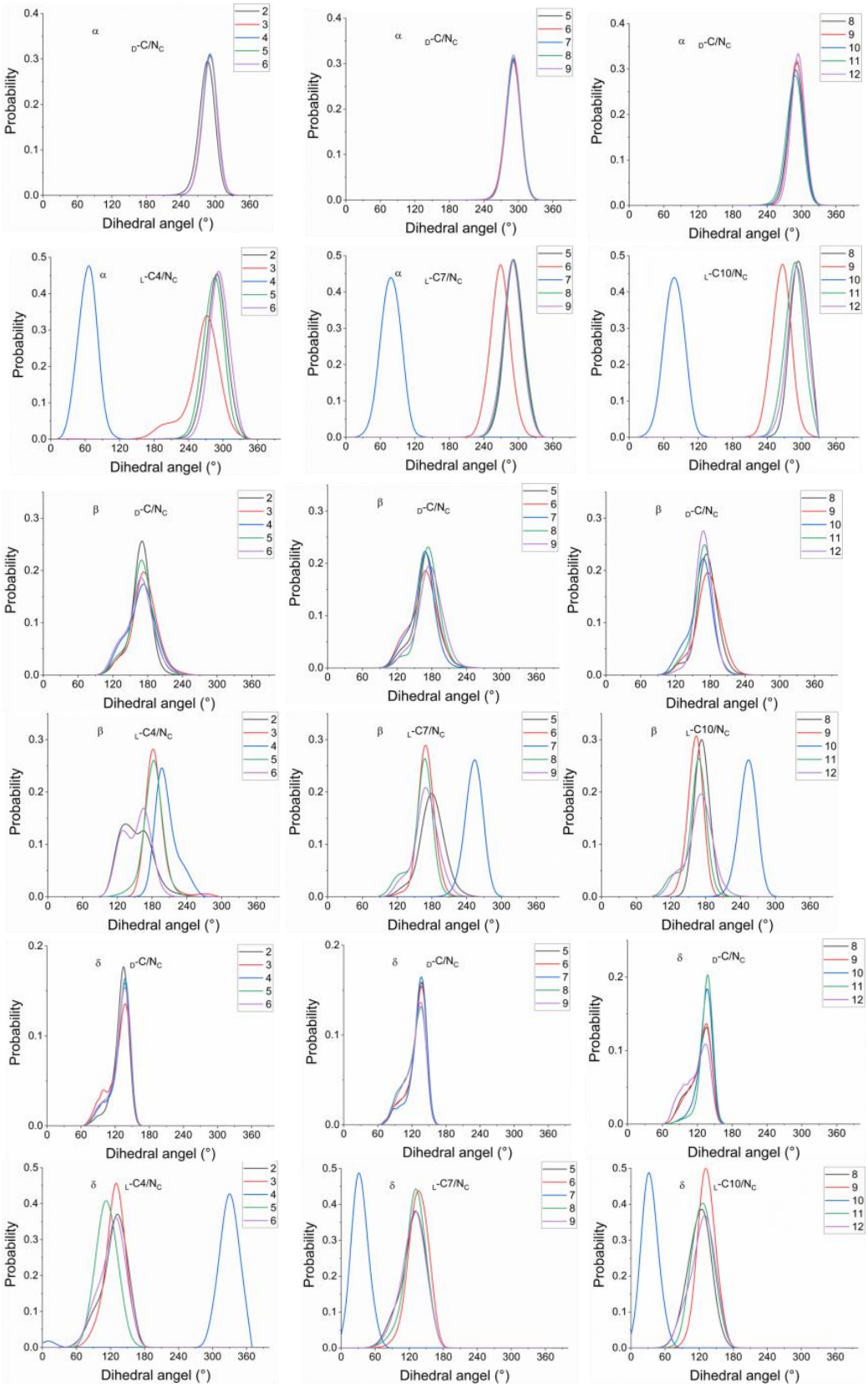
α D-C/NC
α L-C4/NC
α L-C7/NC
α L-C10/NC
β D-C/NC
β L-C4/NC
β L-C7/NC
β L-C10/NC
δ D-C/NC
δ L-C4/NC
δ L-C7/NC
δ L-C10/NC
Probability
Dihedral angel (°)

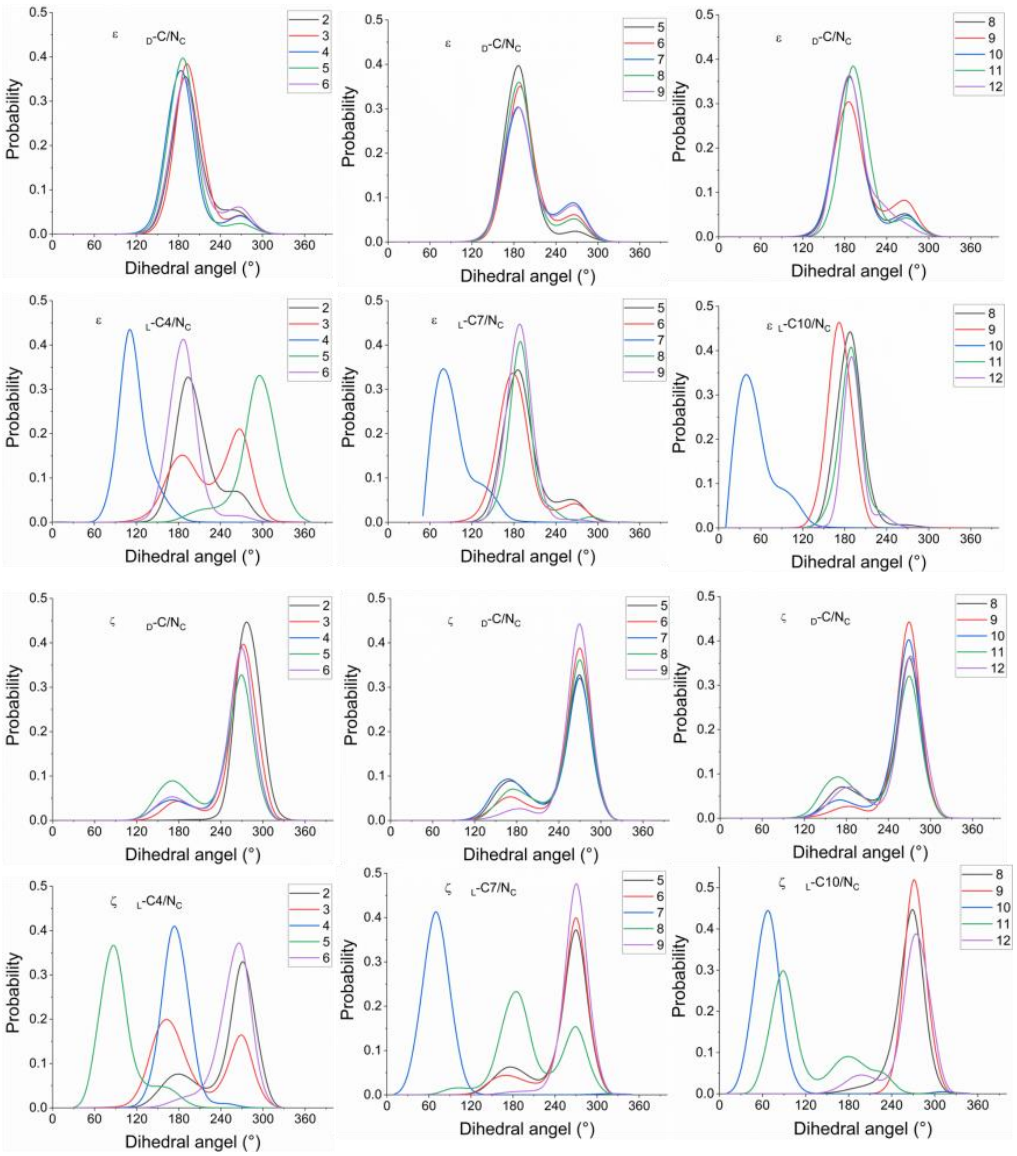

Figure S6c Probability distributions of dihedral angles for L-deoxynucleotides and surrounding deoxynucleotides in the L-dC4/N_C, L-dC7/N_C and L-dC10/N_C.

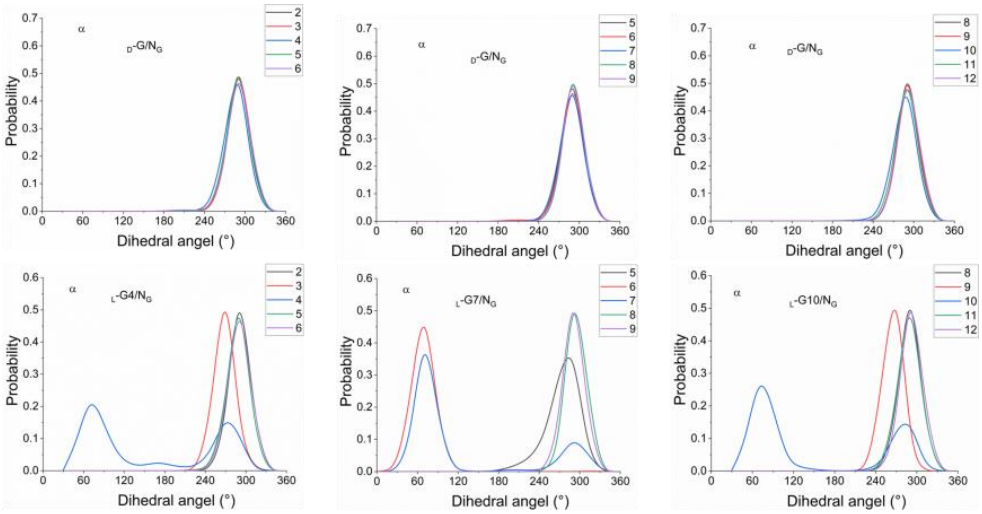

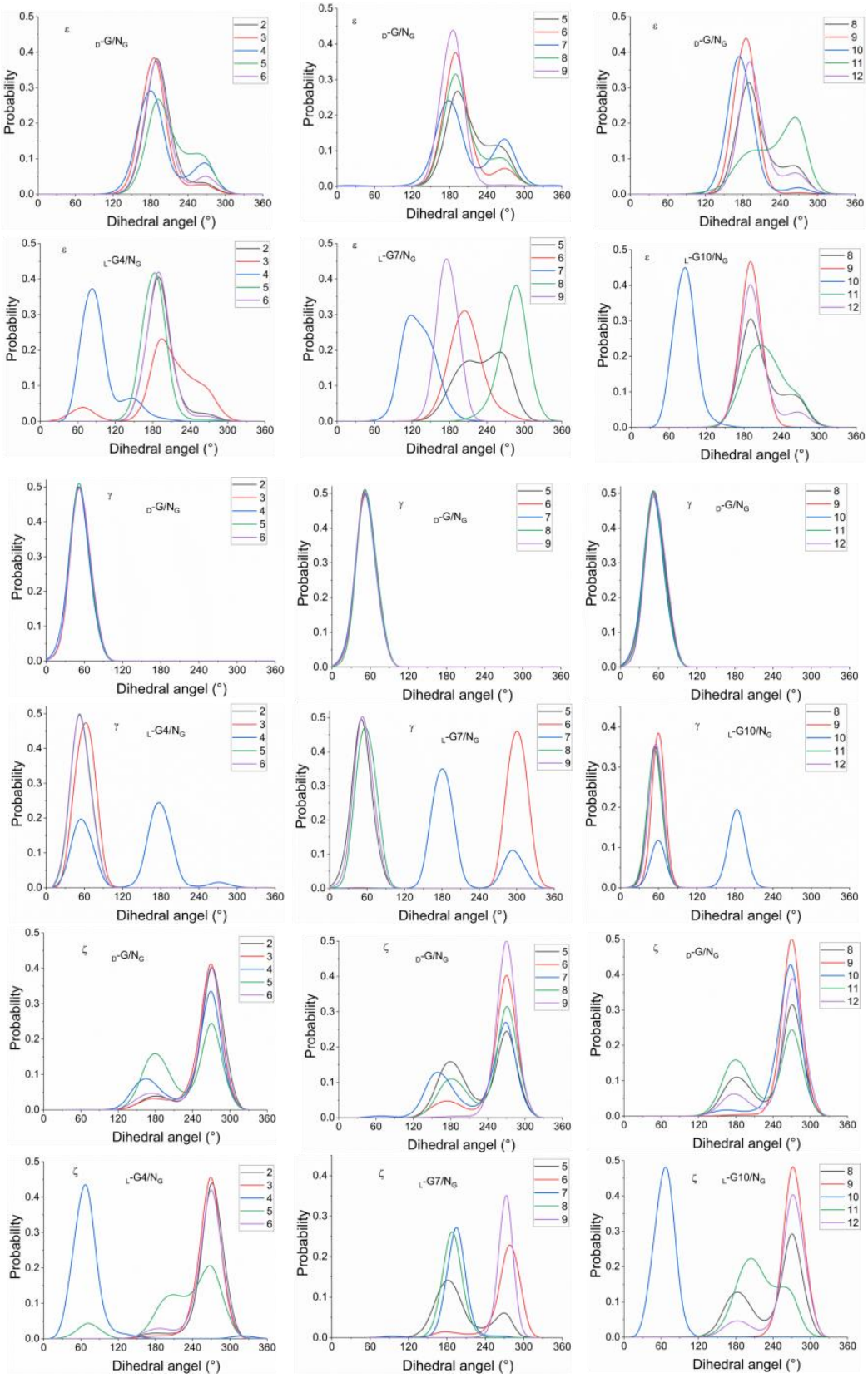

Figure S6d Probability distributions of dihedral angles for L-deoxynucleotides and surrounding deoxynucleotides in the L-dG4/N_G, L-dG7/N_G and L-dG10/N_G.

The helical parameters for DNA−RNA hybrids contaiing L-deoxynucleotides

Table S2 Average helical parameters over the last 10 ns of the MD trajectories for all the duplexes in the study.

Helicoidal parameters	X-disp (Å)	Y-disp (Å)	Rise (Å)	Inclination (°)	Tip (°)	Twist (°)
A form	5	0	2.58	20	0	32
B form	0	0	3.36	0	0	36
$_{D}$-T/N$_{T}$	3.834	-0.075	2.868	8.055	-1.107	33.093
$_{L}$-T4/N$_{T}$	-0.084±2.921	-0.084±0.117	3.006±0.143	8.488±2.616	-1.036±0.964	32.977±0.28
$_{L}$-T7/N$_{T}$	-0.284±2.69	-0.221±0.13	3.016±0.096	7.763±1.088	0.214±1.433	33.762±0.637
$_{L}$-T10/N$_{T}$	-0.19±2.832	-0.329±0.12	3.155±0.141	5.758±1.796	0.424±0.535	32.526±1.141
$_{D}$-A/N$_{A}$	3.969	-0.137	3.012	8.322	-0.132	32.507
$_{L}$-A4/N$_{A}$	-0.339±3.110	-0.192±0.019	2.989±0.044	10.336±2.539	-0.177±0.373	32.421±1.553
$_{L}$-A7/N$_{A}$	-0.141±2.34	-0.503±0.377	3.119±0.132	9.239±2.85	1.095±3.029	32.873±0.423
$_{L}$-A10/N$_{A}$	-0.126±2.852	0.286±0.288	3.069±0.071	7.207±0.88	-2.891±1.297	32.061±0.253
$_{D}$-C/N$_{C}$	3.982	-0.054	3.019	8.659	-0.716	31.746
$_{L}$-C4/N$_{C}$	-0.287±3.561	-0.018±0.106	3.025±0.136	7.694±5.02	0.675±2.406	31.729±2.531
$_{L}$-C7/N$_{C}$	0.098±2.888	-0.168±0.413	3.022±0.243	6.771±1.799	-0.499±0.823	29.309±4.867
$_{L}$-C10/N$_{C}$	0.25±3.128	-0.309±0.116	3.094±0.147	7.924±5.456	0.979±1.494	32.924±1.683
$_{D}$-G/N$_{G}$	3.679	-0.106	2.945	8.007	-0.227	32.001
$_{L}$-G4/N$_{G}$	0.089±2.811	-0.104±0.264	2.981±0.197	7.954±6.079	-0.906±2.088	36.917±4.405
$_{L}$-G7/N$_{G}$	0.133±2.603	-0.117±0.104	3.058±0.276	9.03±2.103	1.596±2.424	33.531±1.45
$_{L}$-G10/N$_{G}$	-0.207±2.797	-0.269±0.163	2.938±0.128	10.035±1.875	-0.064±1.495	33.148±1.284

The Watson-Crick hydrogen bonding occupancy of DNA/RNA hybrids

Table S3a Watson -Crick hydrogen bonding occupancy calculated for $_{D}$-T/N_T, $_{L}$-T4/N_T, $_{L}$-T7/N_T, $_{L}$-T10/N_T over the last 10 ns of the MD trajectories.

Occupacy	$_{D}$-T/N_T	$_{L}$-T4/N_T	$_{L}$-T7/N_T	$_{L}$-T10/N_T
1(N3-N1)	0.6281	0.6275	0.6296	0.6287
1(O2-N2)	0.7909	0.7887	0.792	0.796
1(O6-N4)	0.5826	0.5821	0.5873	0.5869
2(N3-N1)	0.6835	0.6593	0.685	0.6717
2(O2-N2)	0.8156	0.7968	0.8145	0.7973
2(O6-N4)	0.6693	0.6519	0.6688	0.653
3(N3-N1)	0.6867	0.6693	0.6947	0.6736
3(O2-N2)	0.7971	0.7431	0.7893	0.7878
3(O6-N4)	0.6546	0.6194	0.6658	0.6393
4(N3-N1)	0.6699		0.6345	0.6531
4(O4-N6)	0.5773		0.5984	0.5988
5(N3-N1)	0.6987	0.6895	0.6736	0.6904
5(O2-N2)	0.8236	0.7159	0.806	0.8176
5(O6-N4)	0.6488	0.6563	0.6151	0.626
6(N3-N1)	0.6688	0.6504	0.6477	0.6698
6(O2-N2)	0.8011	0.8595	0.6716	0.7898
6(O6-N4)	0.6455	0.5922	0.6469	0.6425
7(N1-N3)	0.6688	0.1902		0.6502
7(O4-N6)	0.5436	0.5579		0.5498
8(N1-N3)	0.7389	0.745	0.5747	0.6183
8(O4-N6)	0.4794	0.4011	0.7034	0.5752
9(N3-N1)	0.7112	0.711	0.6503	0.584
9(O2-N2)	0.79	0.7812	0.9175	0.7972
9(O6-N4)	0.6112	0.5801	0.5035	0.5265
10(N1-N3)	0.6538	0.662	0.7256	
10(O4-N6)	0.4975	0.4697	0.5181	
11(N1-N3)	0.6334	0.6026	0.6856	0.3486
11(O4-N6)	0.3371	0.3931	0.4277	0.3255
12(N1-N3)	0.629	0.6656	0.4515	0.666
12(O4-N6)	0.5769	0.5433	0.6962	0.5054
13(N3-N1)	0.6702	0.6595	0.6901	0.6284
13(O2-N2)	0.7891	0.7752	0.7898	0.7748
13(O6-N4)	0.6166	0.5937	0.6213	0.6058
14(N1-N3)	0.6811	0.6808	0.6716	0.65
14(O4-N6)	0.5696	0.5455	0.5614	0.596
15(N3-N1)	0.6708	0.6688	0.6848	0.6622
15(O2-N2)	0.8049	0.7927	0.8062	0.7977

15(O6-N4)	0.633	0.6195	0.6312	0.6121
16(N1-N3)	0.6996	0.6723	0.6895	0.6847
16(O2-N2)	0.828	0.8028	0.8195	0.8015
16(O6-N4)	0.6667	0.6411	0.669	0.6616
17(N1-N3)	0.3358	0.2952	0.4095	0.1666
17(O4-N6)	0.3033	0.2687	0.3718	0.4235

Table S3b Watson -Crick hydrogen bonding occupancy calculated for $_{D}$-A/N_A, $_{L}$-A4/N_A, $_{L}$-A7/N_A, $_{L}$-A10 /N_A over the last 10 ns of the MD trajectories.

Occupancy	$_{D}$-A/N_A	$_{L}$-A4/N_A	$_{L}$-A7/N_A	$_{L}$-A10/N_A
1(N3-N1)	0.6285	0.6347	0.6238	0.2651
1(O2-N2)	0.7982	0.7929	0.8038	0.7025
1(O6-N4)	0.5872	0.6044	0.5769	0.847
2(N3-N1)	0.6806	0.6731	0.6867	0.6502
2(O2-N2)	0.7698	0.7901	0.7917	0.7
2(O6-N4)	0.6597	0.6672	0.6344	0.8155
3(N3-N1)	0.6424	0.6529	0.6966	0.6624
3(O2-N2)	0.7398	0.7779	0.7608	0.6346
3(O6-N4)	0.6595	0.6566	0.6191	0.5828
4(N1-N3)	0.7297		0.6121	0.7289
4(O4-N6)	0.3301		0.5163	0.6704
5(N3-N1)	0.6404	0.6893	0.6823	0.8636
5(N4-O6)	0.6779	0.6414	0.6551	0.6737
5(O2-N2)	0.7905	0.806	0.818	0.6399
6(N3-N1)	0.6627	0.6445	0.6464	0.7777
6(O6-N4)	0.6048	0.6155	0.6075	0.6785
6(O2-N2)	0.8095	0.8113	0.7646	0.4601
7(N1-N3)	0.6429	0.6423		0.6779
7(O4-N6)	0.4878	0.4866		0.5707
8(N1-N3)	0.7065	0.6595		0.6723
8(O4-N6)	0.4113	0.4943		0.8117
9(N3-N1)	0.6583	0.6554	0.6419	0.6416
9(O2-N2)	0.7636	0.7673	0.7676	0.8117
9(O6-N4)	0.5289	0.5367	0.4922	0.6416
10(N1-N3)	0.6959	0.6561	0.4902	
10(O4-N6)	0.3347	0.3015	0.2279	
11(N1-N3)	0.5047	0.5838	0.6231	0.6450
11(O4-N6)	0.6448	0.4947	0.3463	0.4238
12(N1-N3）	0.7319	0.5888	0.474	0.4941
12(O4-N6)	0.4119	0.4993	0.6553	0.6879
13(N3-N1)	0.6655	0.6581	0.6721	0.6751
13(O2-N2)	0.7727	0.774	0.7823	0.7942

13(O6-N4)	0.5802	0.6064	0.607	0.6612
14(N1-N3)	0.6941	0.6674	0.6854	0.7294
14(O4-N6)	0.5299	0.5541	0.5345	0.37
15(N3-N1)	0.6427	0.6412	0.6781	0.6762
15(O2-N2)	0.7844	0.7639	0.7882	0.8273
15(O6-N4)	0.6159	0.6218	0.6112	0.5618
16(N1-N3)	0.6776	0.7001	0.6509	0.6984
16(N4-O6)	0.6678	0.6413	0.6409	0.6698
16(O2-N2)	0.8004	0.784	0.7938	0.7982
17(N1-N3)	0.46789	0.35679	0.4449	0.40834
17(O4-N6)	0.40976	0.3478	0.3884	0.30635

Table S3c Watson -Crick hydrogen bonding occupancy calculated for $_{D}$-C/N_C, $_{L}$-C4/N_C, $_{L}$-C7/N_C, $_{L}$-C10/N_C over the last 10 ns of the MD trajectories.

Occupancy	$_{D}$-C/N_C	$_{L}$-C4/N_C	$_{L}$-C7/N_C	$_{L}$-C10/N_C
1(N1-N3)	0.6313	0.6714	0.6881	0.6695
1(N2-02)	0.7901	0.854	0.8435	0.8459
1(O6-N4)	0.5891	0.6203	0.6361	0.6336
2(N1-N3)	0.6812	0.7127	0.7245	0.7184
2(O2-N2)	0.8086	0.844	0.8614	0.8559
2(O6-N4)	0.6592	0.7009	0.6838	0.7015
3(N1-N3)	0.6918	0.7173	0.7359	0.7174
3(O2-N2)	0.8167	0.7367	0.8463	0.8505
3(O6-N4)	0.6704	0.7225	0.7048	0.6854
4(N1-N3)	0.6962		0.7293	0.7094
4(O2-N2)	0.8133		0.8428	0.8531
4(O6-N4)	0.6535		0.6969	0.6933
5(N1-N3)	0.6869	0.674	0.7138	0.7049
5(N2-O2)	0.8123	0.8601	0.8329	0.8515
5(O6-N4)	0.6551	0.5482	0.6805	0.6859
6(N1-N3)	0.667	0.7157	0.6475	0.7157
6(O2-N2)	0.7961	0.8473	0.6982	0.8441
6(O6-N4)	0.639	0.7068	0.7233	0.7042
7(N1-N3)	0.6625	0.7209		0.6933
7(N2-O2)	0.7603	0.8191		0.8162
7(O6-N4)	0.6774	0.6815		0.6662
8(N1-N3)	0.6757	0.707	0.5784	0.6633
8(O4-N6)	0.5683	0.6023	0.6126	0.585
9(N1-N3)	0.736	0.7522	0.7351	0.4691
9(O2-N2)	0.84	0.869	0.8629	0.4826
9(O6-N4)	0.6323	0.6571	0.6331	0.6996

10(N1-N3)	0.6874	0.7194	0.7376	
10(O2-N2)	0.8117	0.8502	0.8411	
10(O6-N4)	0.616	0.6295	0.633	
11(N1-N3)	0.6294	0.6796	0.6881	0.5794
11(O4-N6)	0.4274	0.4494	0.4613	0.4228
12(N1-N3)	0.6327	0.6158	0.6481	0.6185
12(O4-N6)	0.5471	0.6176	0.5785	0.6501
13(N1-N3)	0.6577	0.6947	0.6913	0.718
13(O2-N2)	0.7794	0.8201	0.8069	0.8364
13(O6-N4)	0.6098	0.6488	0.6448	0.6666
14(N1-N3)	0.675	0.717	0.7256	0.7046
14(O4-N6)	0.57	0.589	0.5507	0.61
15(N1-N3)	0.7052	0.6944	0.749	0.686
15(O2-N3)	0.8138	0.8393	0.8575	0.818
15(O6-N4)	0.6333	0.6284	0.6899	0.6602
16(N1-N3)	0.6755	0.7265	0.703	0.7361
16(O2-N2)	0.8128	0.8561	0.8521	0.8648
16(O6-N4)	0.6544	0.6869	0.6981	0.6834
17(N1-N3)	0.5628	0.4095	0.4724	0.1606
17(O4-N6)	0.4789	0.3678	0.4554	0.1519

Table S3d Watson -Crick hydrogen bonding occupancy calculated for $_{D}$-G/N_G, $_{L}$-G4/N_G, $_{L}$-G7/N_G, $_{L}$-G10/N_G over the last 10 ns of the MD trajectories.

Occupancy	$_{D}$-G/N_G	$_{L}$-G4/N_G	$_{L}$-G7/N_G	$_{L}$-G10/N_G
1(N3-N1)	0.6379	0.6758	0.3682	0.6459
1(O2-N2)	0.8006	0.8565	0.1917	0.8204
1(O6-N4)	0.611	0.6371	0.6487	0.6051
2(N1-N3)	0.6852	0.75	0.659	0.6955
2(O2-N2)	0.8167	0.8541	0.7999	0.8275
2(O6-N4)	0.6597	0.6901	0.6512	0.6666
3(N1-N3)	0.6821	0.6839	0.6873	0.7181
3(O2-N2)	0.8038	0.779	0.8055	0.818
3(O6-N4)	0.6379	0.6835	0.6079	0.6615
4(N3-N1)	0.6983		0.703	0.7077
4(O2-N2)	0.8126		0.8058	0.8355
4(O6-N4)	0.6753		0.61	0.6813
5(N1-N3)	0.7118	0.7598	0.6299	0.726
5(O2-N2)	0.8329	0.8695	0.8211	0.8524
5(O6-N4)	0.672	0.7421	0.598	0.6986
6(N1-N3)	0.6611	0.7119	0.6181	0.6668
6(O2-N2)	0.7876	0.8252	0.6128	0.8124

6(O6-N4)	0.6471	0.6917	0.6636	0.6594
7(N3-N1)	0.6662	0.7058		0.6945
7(O2-N2)	0.809	0.8497		0.8342
7(O6-N4)	0.6583	0.7141		0.6735
8(N1-N3)	0.6869	0.7141	0.4379	0.7072
8(O4-N6)	0.5521	0.5751	0.6137	0.5447
9(N3-N1)	0.6808	0.7349	0.6723	0.6837
9(O2-N2)	0.8168	0.8663	0.8131	0.6613
9(O6-N4)	0.5363	0.5405	0.4694	0.5619
10(N3-N1)	0.695	0.7268	0.6864	
10(O2-N2)	0.8129	0.8527	0.8181	
10(O6-N4)	0.5679	0.5701	0.5265	
11(N1-N3)	0.6692	0.719	0.6657	0.6187
11(O4-N6)	0.2651	0.2523	0.191	0.4673
12(N1-N3)	0.5474	0.5577	0.4644	0.6289
12(O4-N6)	0.6426	0.704	0.6893	0.5686
13(N3-N1)	0.6561	0.7007	0.653	0.6584
13(O2-N2)	0.7877	0.7772	0.7756	0.7999
13(O6-N4)	0.6202	0.6645	0.6028	0.6051
14(N1-N3)	0.6604	0.7449	0.654	0.6992
14(O4-N6)	0.6073	0.3897	0.5523	0.5403
15(N1-N3)	0.6806	0.7213	0.6584	0.7092
15(O2-N2)	0.8102	0.8646	0.7694	0.8208
15(O6-N4)	0.5989	0.5878	0.6042	0.6518
16(N1-N3)	0.7158	0.6994	0.6639	0.696
16(O2-N2)	0.811	0.837	0.7998	0.8229
16(O6-N4)	0.6315	0.6671	0.6356	0.6726
17(N1-N3)	0.2925	0.3672	0.448	0.5202
17(O4-N6)	0.2547	0.3209	0.3941	0.4582

The hydrogen bonding occupancy of L-deoxynucleotides in the different sites of DNA-RNA hybrids.

Table S4a L-dT hydrogen bonding occupancy calculated over the last 10 ns of the MD trajectories

Nucleotide	Occupancy
L-dT4/N_T	
N3(L-dT4)·····O2(dC6)	0.4419
O2(L-dT4)·····N2(rG6)	0.2808
N3(L-dT4)·····N3(dT7)	0.1902
OP2(L-dT4)·····N4(dC3)	0.1802
L-dT7/N_T	
N3(L-dT7)·····N3(dT10)	0.2391
N3(L-dT7)·····O2(dC9)	0.2238
O2(L-dT7)·····N2(rG9)	0.3607
OP2(L-dT7)·····N4(dC6)	0.3326

Table S4b L-dA hydrogen bonding occupancy calculated over the last 10 ns of the MD trajectories

Nucleotide	Occupancy
L-dA4/N_A	
L-dA4(N7)·····rU4(N3)	0.6053
L-dA4(N6)·····rU4(O4)	0.3541
L-dA7/N_A	
dT8(O4)·····rU7(N3)	0.6976
dT8(N3)·····rU7(O2)	0.3889
L-dA10/N_A	
L-dA10(N7)·····rU10(N3)	0.692
L-dA10(N6)·····rU10(O4)	0.5973

Table S4c $_{L}$-dC hydrogen bonding occupancy calculated over the last 10 ns of the MD trajectories.

Nucleotide	Occupancy
$_{L}$-dC4/N_C	
$_{L}$-dC4(N4) ·····rG6(O4')	0.3731
$_{L}$-dC4(N4) ·····rG5(N2)	0.1754
$_{L}$-dC7/N_C	
$_{L}$-dC7(N4) ·····rG7(O6)	0.4186
$_{L}$-dC7(N3) ·····rG7(N2)	0.6618
$_{L}$-dC10/N_C	
$_{L}$-dC10(N4) ·····rG10(O6)	0.5641
$_{L}$-dC10(N3) ·····rG10(N2)	0.3727

Table S4d $_{L}$-dG hydrogen bonding occupancy calculated over the last 10 ns of the MD trajectories.

Nucleotide	Occupancy
$_{L}$-dG4/N_G	
$_{L}$-dG4(N2) ·····rC4(N3)	0.6142
$_{L}$-dG4(N1) ·····rC4(O2)	0.8062
$_{L}$-dG7/N_G	
$_{L}$-dG7(N2) ·····rC10(O2)	0.1236
$_{L}$-dG7(N2) ·····dC9(O2)	0.2472
$_{L}$-dG7(N1) ·····dG10(N2)	0.2720
$_{L}$-dG10/N_G	
$_{L}$-dG10(N2) ·····rC10(N3)	0.4757
$_{L}$-dG10(N1) ·····rC10(O2)	0.5831

Structure details about $_L$-deoxynucleotides in the different DNA/RNA hybrid systems

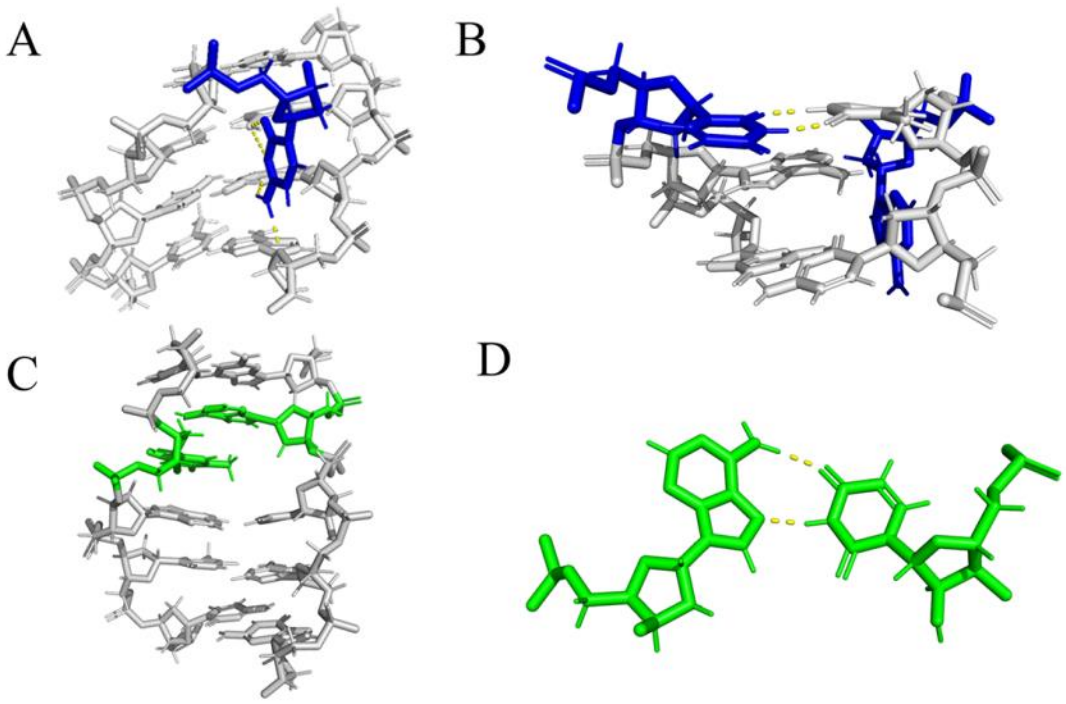

Figure S7 Hydrogen bond details about $_L$-deoxynucleotides in the different systems. (A) distortion ($_L$-T4/N_T, $_L$-T7/N_T, $_L$-A7/N_A,

The root means square fluctuation (RMSF) values for all the duplexes containing L-deoxyribonucleoside

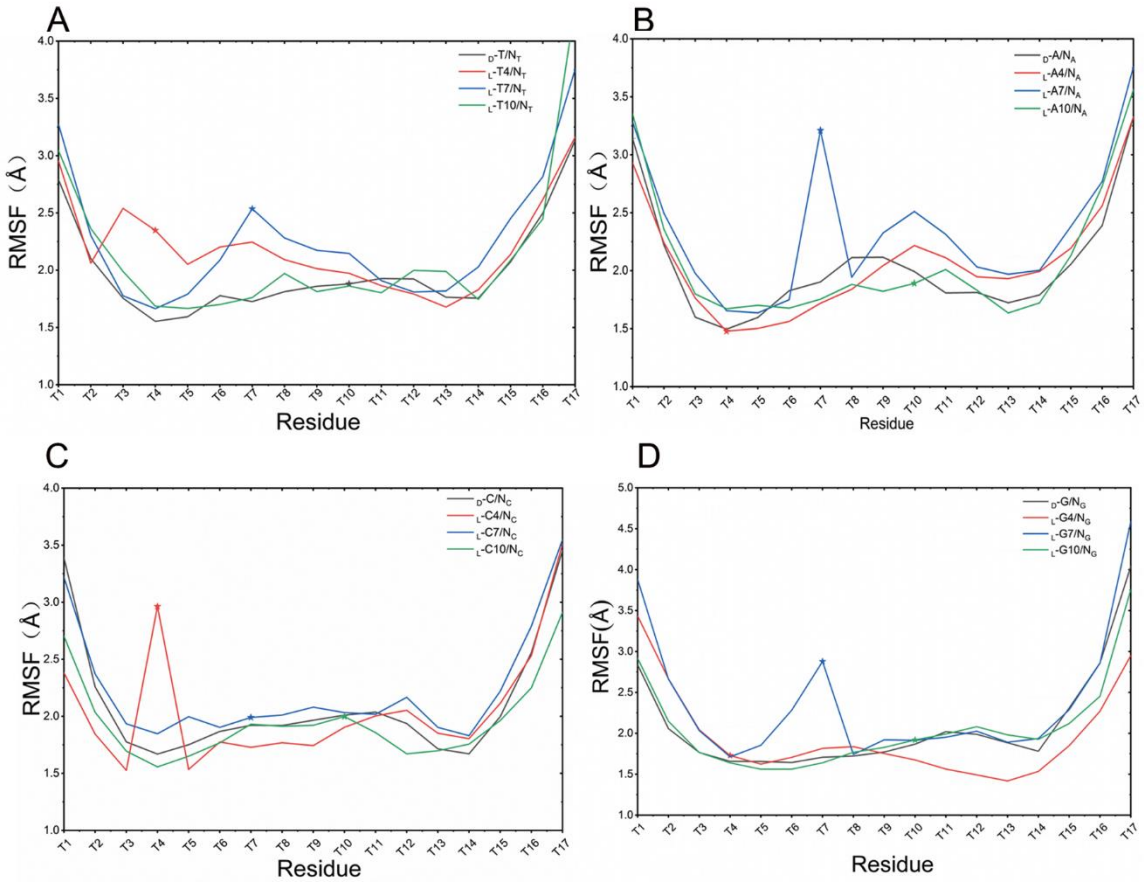

Figure S8 The Root-Mean-Square Fluctuation (RMSF) values of each residue in the modified or unmodified DNA/RNA hybrids. Tn corresponds to the residue at n position of DNA template.

Relative binding energies for DNA−RNA hybrids containing L-dA, L-dT, L-dC and L-dG

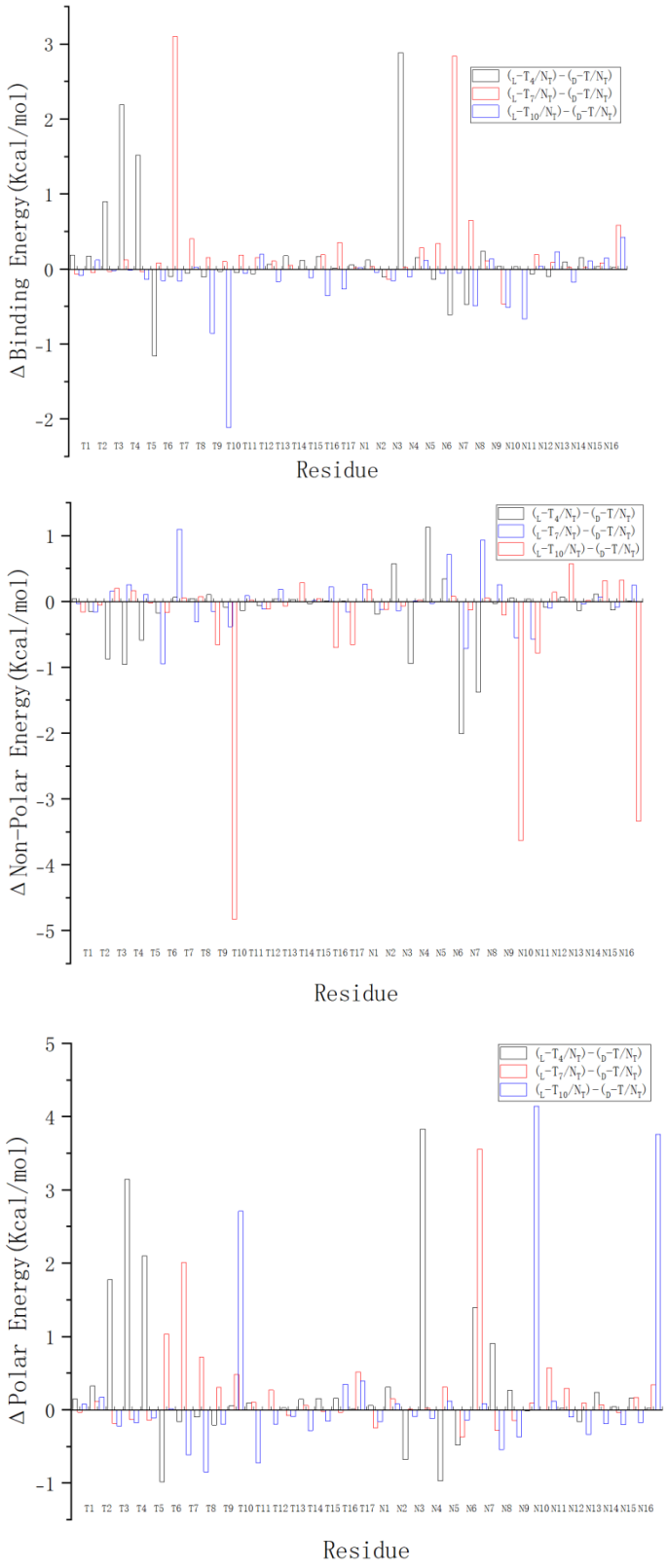

Figure S9 Relative binding energies (kcal/mol) for DNA−RNA hybrids with incorporated L-dT at the different positions of template chain.

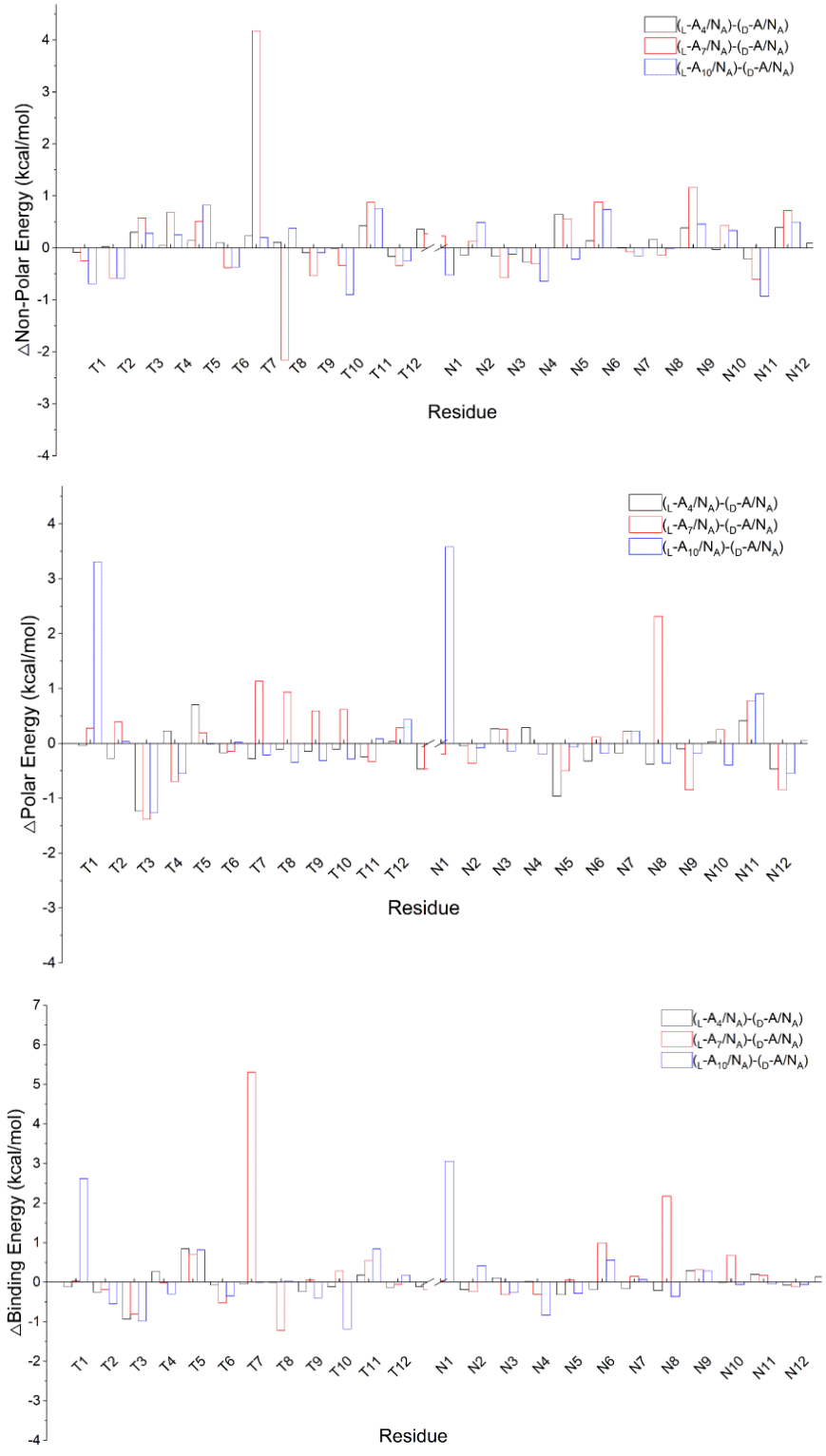

Figure S10 Relative binding energies for DNA−RNA hybrids with incorporated L-dA at the different positions of template chain.

.

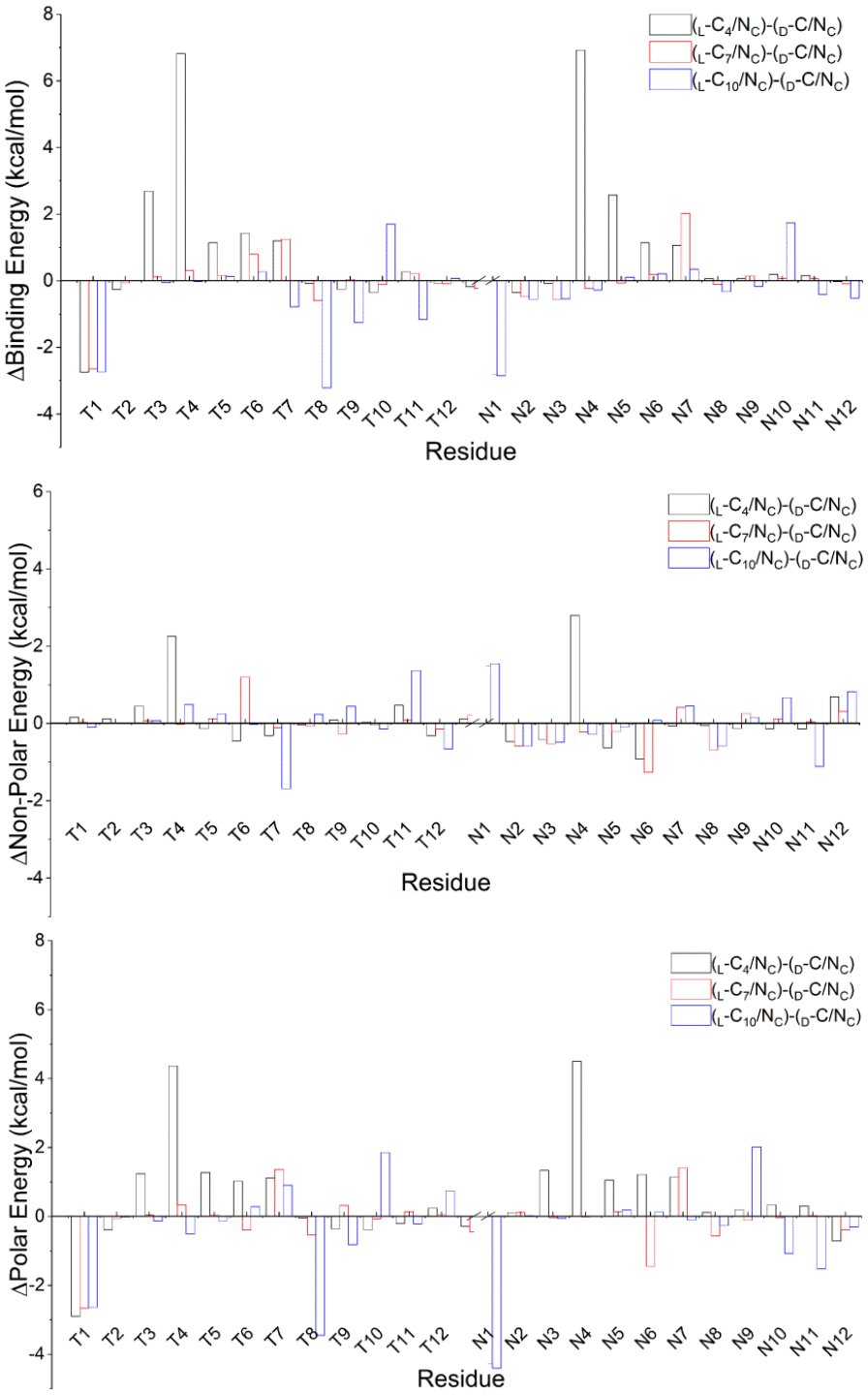

Figure S11 Relative binding energies for DNA−RNA hybrids with incorporated $_{L}$-dC at the different positions of template chain.

.

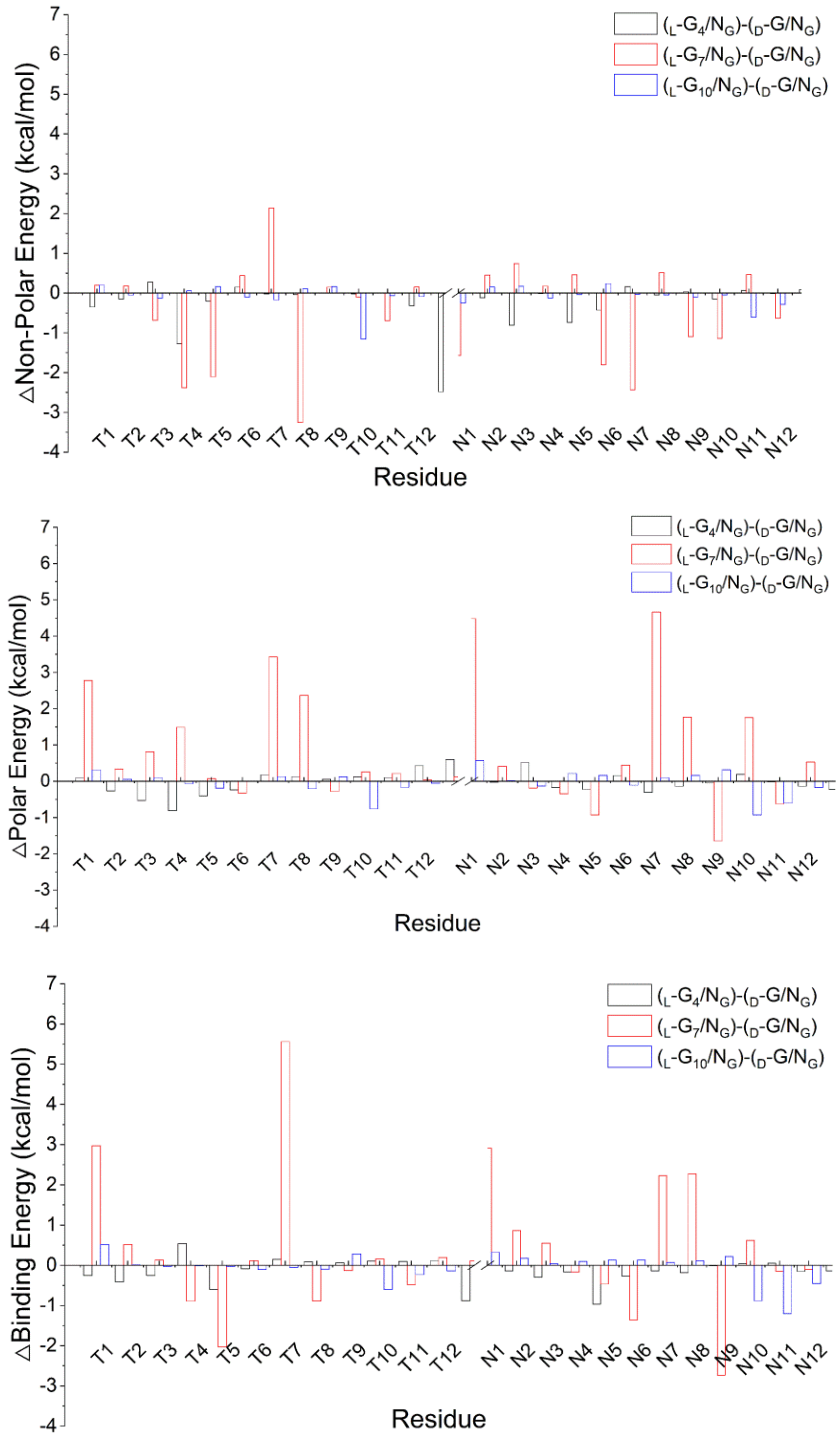

Figure S12 Relative binding energies for DNA−RNA hybrids with incorporated $_L$-dG at the different positions of template chain.

.

The hydrogen bonding interactions calculated for T7RNA polymerase complex

Table S5 Hydrogen bonding occupancy between template bases and active center of T7RNA polymerase.

Hydrogen Bond	Occupacy
Glu338(OE1)·····dT24(N3)	0.906
Arg336(O)·····dC26(N4)	0.734
Glu554(OE1)·····dT28(N3)	0.709
Arg189(O)·····dG19(N2)	0.402
Asn187(OD1)·····dG19(N2)	0.377
Asn187(OD1)·····dG19(N1)	0.365
Asn187(O)·····dG19(N2)	0.307
Tyr550(OH)·····rU18(O2')	0.207
Ser354(OG)·····rC43(N2)	0.206
Asn97(OD1)·····rC40(N4)	0.19
Lys542(O)·····rU18(O2')	0.163
Gln558(OE1)·····dA11(N6)	0.103

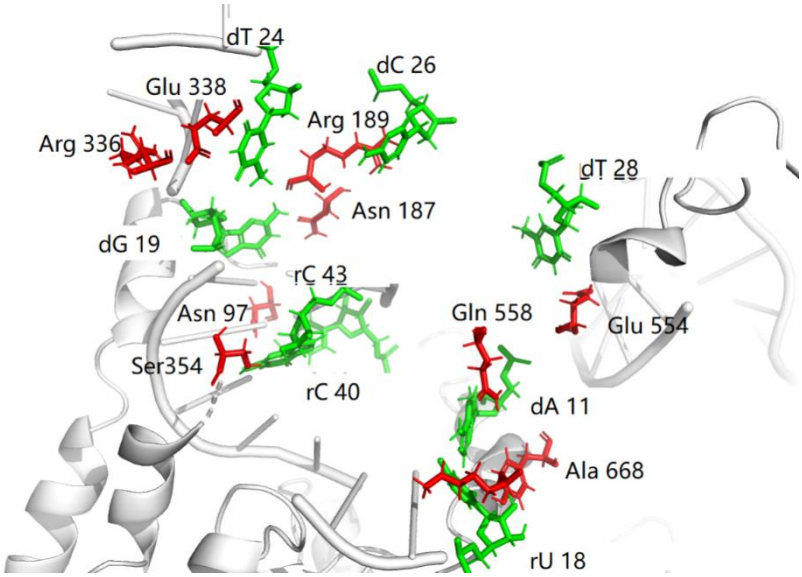

Figure S13 The hydrogen bonding between template bases and active center of T7 RNA polymerase.

Root mean square deviation

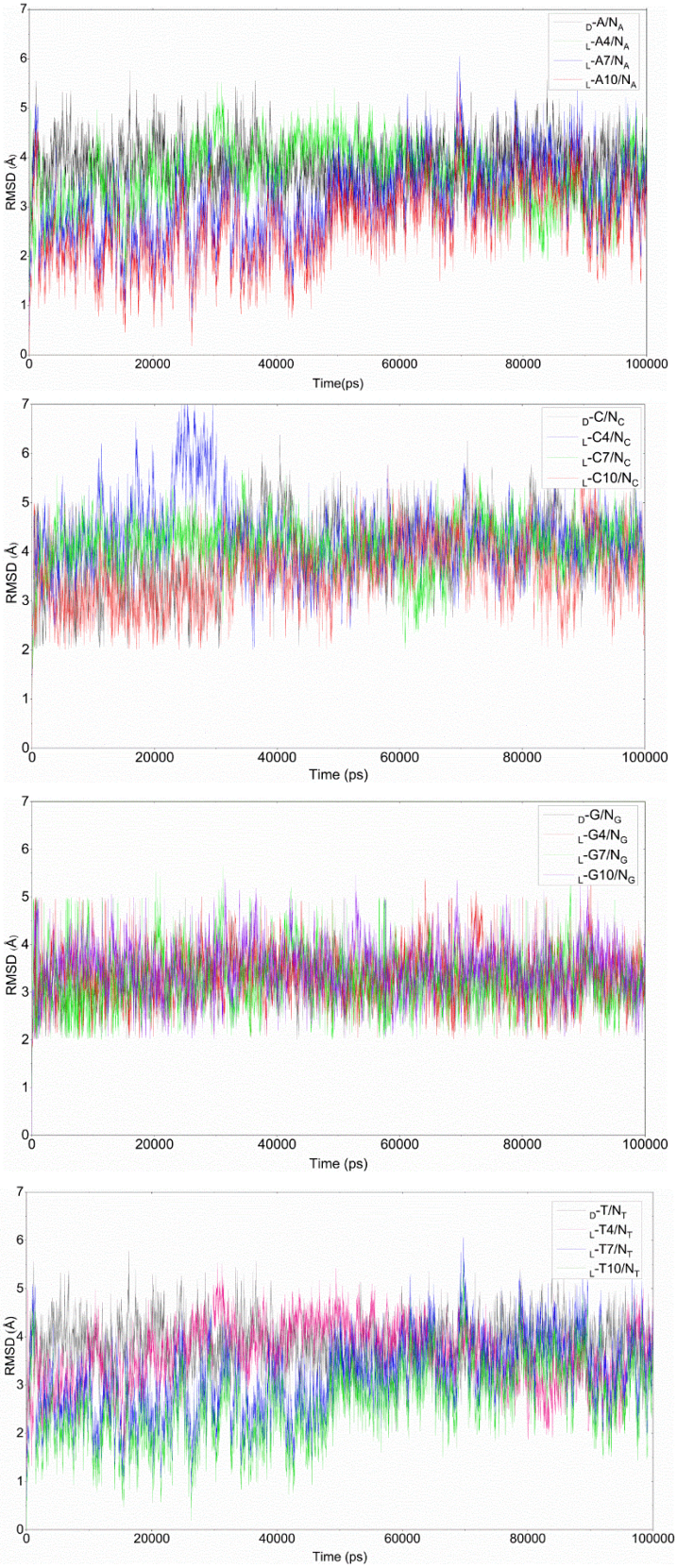

Figure S14 RMSD of the L-deoxynucleoside modified DNA-RNA hybrid duplexes.

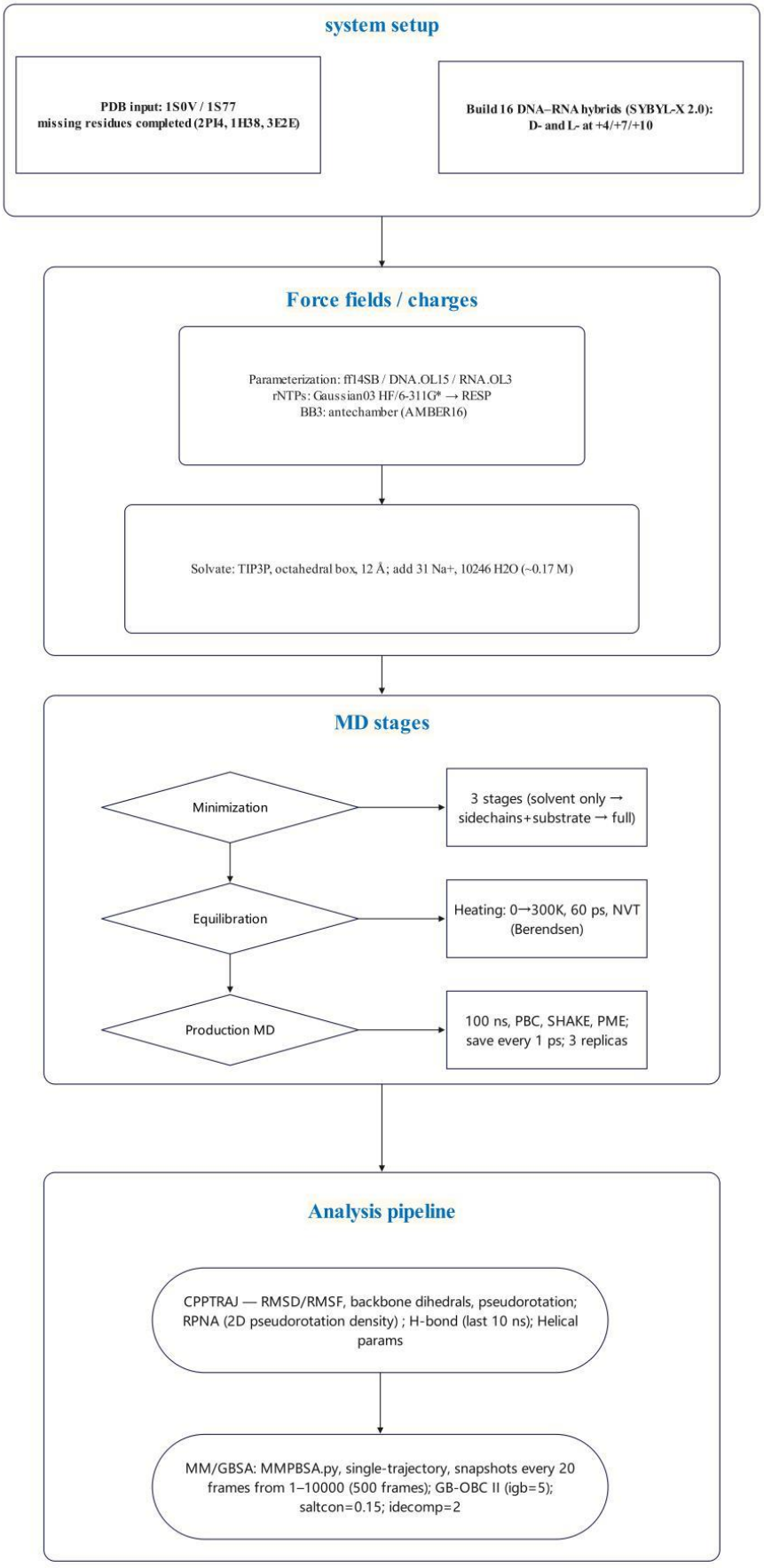
system setup
PDB input: 1S0V / 1S77
missing residues completed (2PI4, 1H38, 3E2E)
Build 16 DNA–RNA hybrids (SYBYL-X 2.0):
D- and L- at +4/+7/+10
Force fields / charges
Parameterization: ff14SB / DNA.OL15 / RNA.OL3
rNTPs: Gaussian03 HF/6-311G* → RESP
BB3: antechamber (AMBER16)
Solvate: TIP3P, octahedral box, 12 Å; add 31 Na+, 10246 H2O (~0.17 M)
MD stages
Minimization
3 stages (solvent only → sidechains+substrate → full)
Equilibration
Heating: 0→300K, 60 ps, NVT (Berendsen)
Production MD
100 ns, PBC, SHAKE, PME; save every 1 ps; 3 replicas
Analysis pipeline
CPPTRAJ — RMSD/RMSF, backbone dihedrals, pseudorotation; RPNA (2D pseudorotation density) ; H-bond (last 10 ns); Helical params
MM/GBSA: MMPBSA.py, single-trajectory, snapshots every 20 frames from 1–10000 (500 frames); GB-OBC II (igb=5); saltcon=0.15; idecomp=2

Figure S15 Schematic workflow for MD simulations and analysis used in this work. Structures of T7 RNAP (1S0V and 1S77) were repaired and modified (SYBYL-X) to introduce L-deoxynucleotides at positions +4/+7/+10 and to build 16 DNA–RNA hybrids. Systems were protonated with tleap and parameterized using ff14SB (protein), DNA.OL15 (DNA) and RNA.OL3 (RNA); rNTPs were optimized at HF/6-311G* and RESP charges assigned (Gaussian03/Amber16); BB3 parameters were prepared with an techamber. Each solvated system (TIP3P, octahedral box, 12 Å, ~0.17 M Na^+) underwent three-stage minimization, heating 0→300 K in 60 ps (NVT, Berendsen), and 100-ns production MD (SHAKE, PME; frames saved every 1 ps). For each complex three independent replicas were run. Trajectory analyses included RMSD/RMSF, backbone dihedrals and pseudorotation angles (used to build the RPNA, Ramachandran-like plot), hydrogen-bond statistics (last 10 ns), helical parameters, and MM/GBSA free-energy calculations (MMPBSA.py, single-trajectory, igb=5, saltcon=0.15; snapshots every 20 frames from frame 1–10000 → 500 frames; residue-pair decomposition idecomp=2). These structural and energetic analyses were combined to classify local nucleotide geometries (distorted, dislocated, π-π stacked, non-Watson-Crick) and to relate them to observed transcriptional activity.